catalysts

MDPI

Article

Controllable Synthesis of Fe_2O_3/Nickel Cobaltite Electrocatalyst to Enhance Oxidation of Small Molecules

Fowzia S. Alamro [1], Shymaa S. Medany [2,*], Nada S. Al-Kadhi [1], Ayman M. Mostafa [3,4], Walaa F. Zaher [5], Hoda A. Ahmed [2,6] and Mahmoud A. Hefnawy [2,*]

[1] Department of Chemistry, College of Science, Princess Nourah bint Abdulrahman University, P.O. Box 84428, Riyadh 11671, Saudi Arabia
[2] Chemistry Department, Faculty of Science, Cairo University, Giza 12613, Egypt
[3] Department of Physics, College of Science, Qassim University, Buraidah 51452, Saudi Arabia
[4] Spectroscopy Department, Physics Research Institute, National Research Centre, Dokki, Giza 12622, Egypt
[5] Department of Chemistry, College of Science, University of Bisha, Bisha 61922, Saudi Arabia
[6] Chemistry Department, Faculty of Science at Yanbu, Taibah University, Yanbu 46423, Saudi Arabia
* Correspondence: shymaasamir80@cu.edu.eg or shymaa@sci.cu.edu.eg (S.S.M.); maahefnawy@gmail.com or maadel@cu.edu.eg (M.A.H.)

Abstract: Nickel-based catalysts have been widely recognized as highly promising electrocatalysts for oxidation. Herein, we designed a catalyst surface based on iron oxide electrodeposited on $NiCo_2O_4$ spinel oxide. Nickel foam was used as a support for the prepared catalysts. The modified surface was characterized by different techniques like electron microscopy and X-ray photon spectroscopy. The activity of the modified surface was investigated through the electrochemical oxidation of different organic molecules such as urea, ethanol, and ethylene glycol. Therefore, the modified Fe@ $NiCo_2O_4$/NF current in 1.0 M NaOH and 1.0 M fuel concentrations reached 31.4, 27.1, and 17.8 mA cm^{-2} for urea, ethanol, and ethylene glycol, respectively. Moreover, a range of kinetic characteristics parameters were computed, such as the diffusion coefficient, Tafel slope, and transfer coefficient. Chronoamperometry was employed to assess the electrode's resistance to long-term oxidation. Consequently, the electrode's activity exhibited a reduction ranging from 17% to 30% over a continuous oxidation period of 300 min.

Keywords: spinel oxide; fuel cell; urea oxidation; ethylene glycol oxidation; ethanol oxidation

Citation: Alamro, F.S.; Medany, S.S.; Al-Kadhi, N.S.; Mostafa, A.M.; Zaher, W.F.; Ahmed, H.A.; Hefnawy, M.A. Controllable Synthesis of Fe_2O_3/Nickel Cobaltite Electrocatalyst to Enhance Oxidation of Small Molecules. *Catalysts* **2024**, *14*, 329. https://doi.org/10.3390/catal14050329

Academic Editors: Loreta Tamasauskaite-Tamasiunaite and Virginija Kepeniene

Received: 23 April 2024
Revised: 9 May 2024
Accepted: 14 May 2024
Published: 17 May 2024

1. Introduction

Fossil fuel has served as the primary energy source for approximately one century. There has been a notable surge in the oil production rate, with projections indicating a potential demand of approximately 16 million tons per day by 2030. This surge can be attributed to the substantial growth observed in industrial development and the global population. Therefore, ongoing research primarily focuses on substituting conventional fossil fuels with sustainable and environmentally friendly energy sources [1–4].

A fuel cell is an electrochemical apparatus that directly converts chemical energy into electrical energy. The fundamental component responsible for converting chemical energy into electrical energy in fuel cells is known as the unit cell. The system comprises an electrolyte near an anode, which serves as the negative electrode, and a cathode, which functions as the positive electrode [5–7]. Noble metal surfaces, specifically platinum (Pt), gold (Au), and palladium (Pd), have predominantly been employed for electro-oxidation applications [8–11]. Most researchers have focused on examining the electro-oxidation of small molecules on cost-effective surfaces or, at the very least, on surfaces modified with noble metals to minimize expenses while maintaining electrode activity [12,13].

Spinel oxides, characterized by the general formula AB_2O_4, where A and B represent elements such as Co, Cu, Mn, Ni, and others, have been conventionally examined as anodes

for fuel cell application [14–16]. In recent years, scholars have commenced contemplating the utilization of spinel oxides as potential anode materials in fuel cells [17–19]. Nickel cobaltite, as a spinel oxide, is extensively employed in energy-related purposes like direct fuel cells, capacitors, and hydrogen production [20–25].

Nickel cobaltite ($NiCo_2O_4$) has garnered significant attention, and substantial research has been dedicated to exploring its electrochemical uses like the electrochemical oxidation of small molecules. Ding et al. reported on the use of mesoporous spinel $NiCo_2O_4$ for the conversion of urea in an alkaline medium and showed that the electrode exhibited a current density of 136 mA cm^{-2} g^{-1} at a potential of 0.7 V (vs. Hg/HgO) in a solution containing 1.0 M KOH and 0.33 M urea. Additionally, the electrode demonstrated satisfactory stability [26]. Furthermore, a hierarchical $NiCo_2O_4$ nanowire array supported on Ni foam was reported by Sha et al. for urea electrochemical oxidation. The $NiCo_2O_4$/NF electrode had a low open potential of 0.19 V vs. Ag/AgCl, along with a current density of 570 mA cm^{-2}. This performance was achieved in electrolytes containing 5.0 M KOH and 0.33 M urea [27]. Additionally, the electrochemical oxidation of ethanol upon nickel cobaltite was reported by Zhan et al, whereas $NiCo_2O_4$/GCE demonstrated much superior electrocatalytic performance, characterized by a larger current density and a lower onset potential, in comparison to both Co_3O_4 and NiO [28].

Iron (Fe) and iron oxide (Fe_2O_3) have been identified as beneficial co-catalysts or supports for metal-based catalysts. These materials offer several advantages over other metal oxides, primarily due to their cost-effectiveness and exceptional physicochemical characteristics. Notably, Fe and Fe_2O_3 exhibit high surface area, porosity, and electropositivity, significantly enhancing the activity of catalysts. Moreover, these properties facilitate electronic and bifunctional mechanisms over electrode surfaces [29,30].

The utilization of nickel foam (NF) electrodes has been proposed as a feasible alternative to platinum-based materials for the electrochemical oxidation of ammonia. The primary reason for this is attributed to their unique three-dimensional porous structure, relatively large specific surface area, impressive mechanical strength, and remarkable corrosion resistance [31,32]. Consequently, nickel foam was reported as a substrate for electrochemical oxidation in materials like CuCo/NF [33], $NiMoO_4$/NF [34], $Ni@Ni_2P$/NF [35], and $NiCo_2S_4$/NF [36]. The electrochemical oxidation of fuel depends on many factors like diffusion, adsorption, and charge transfer. Therefore, designing a more complex electrocatalyst can enhance the adsorption process by using a suitable substrate like nickel foam. Otherwise, the use of binary metals like spinel oxide ($NiCo_2O_4$) enhances the activity due to the diversity of the oxidation state. Additionally, the use of an oxide with a high charge transfer ability like Fe_2O_3 can enhance the activity of fuel oxidation by facilitating the transfer of electrons from the product to the electrode.

In this work, nickel cobalt oxide was supported by nickel foam. Then, the iron oxide was electrodeposited on $NiCo_2O_4$/NF. The presence of Fe_2O_3 enhanced the charge transfer step in electrochemical oxidation upon $NiCo_2O_4$. The use of the electrochemical deposition technique is considered as a controllable method for the preparation of nanoparticles. However, the activity of $Fe@NiCo_2O_4$/NF was characterized by different techniques. Several electrochemistry techniques were employed to judge the performance of the electrode toward the oxidation of urea, ethanol, and ethylene glycol. Various parameters were calculated to confirm the activity of the modified electrode toward fuel oxidation like the diffusion coefficient, surface coverage, and charge transfer resistance.

2. Results Section

2.1. Structural and Surface Characterization

The chemical structure of the prepared $Fe@NiCo_2O_4$/NF was investigated using powder X-ray diffraction. In Figure 1, the XRD chart of the $Fe@NiCo_2O_4$/NF electrode is shown. Thus, three phases of materials can be identified, namely, nickel foam, $NiCo_2O_4$, and Fe_2O_3.

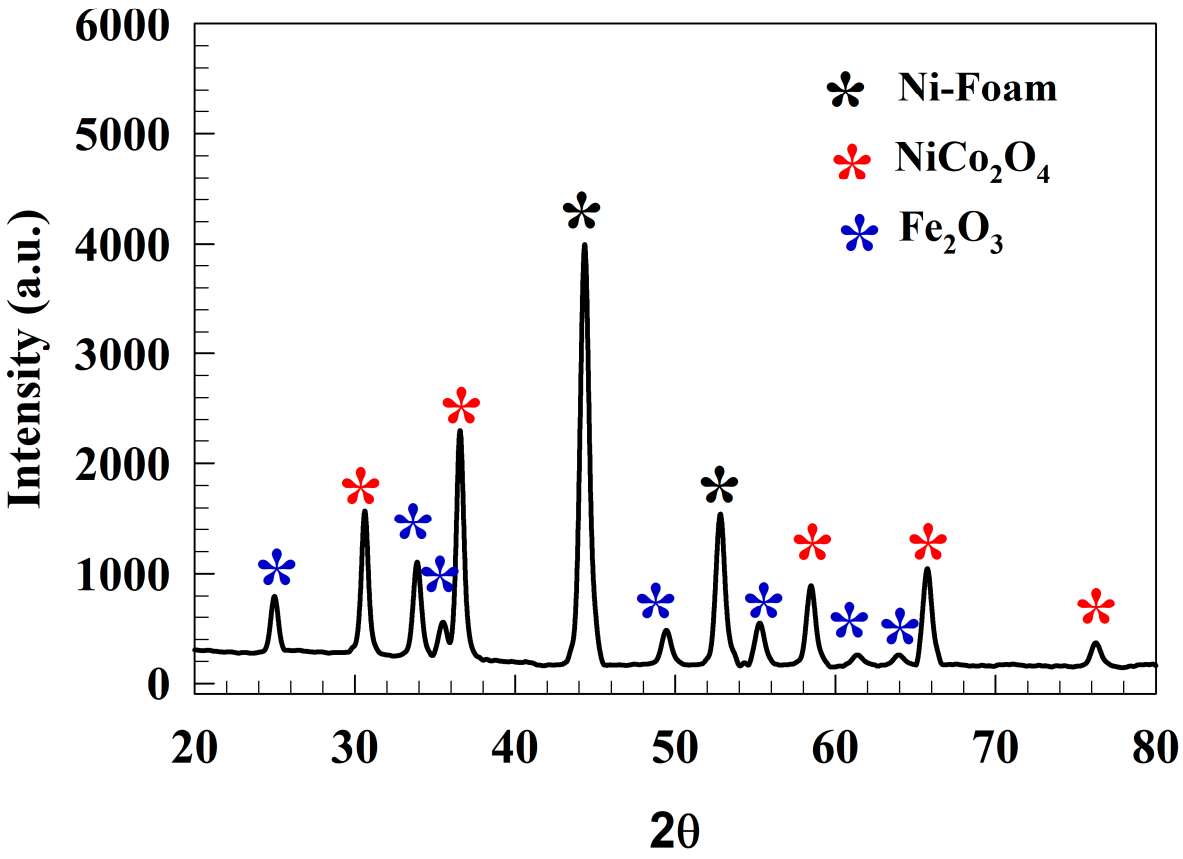

Figure 1. XRD chart for Fe@$NiCo_2O_4$/NF.

The Ni foam, as it is received, exhibits two distinct reflections at angles of 44 and 52°. These reflections correspond to the (111) and (200) reflections of cubic Ni, as defined by the JCPDS No. 004–0850, with a Fm-3m space group [37–39]. The prepared $NiCo_2O_4$ has five clear reflections at angles of 30,4, 36.7, 58.3, 65.8, and 76.4°. The reflections being discussed are the (220), (311), (511), (440), and (533) reflections of cubic $NiCo_2O_4$, as specified by the JCPDS No. 73-1702 [40–42].

The synthesized Fe_2O_3 exhibits seven distinct reflections at angles of 24.6°, 33.9°, 35.4°, 49.1°, 55.1, 62.2, and 64.1°. The reflections under discussion are the (012), (104), (110), (113), (024), (116), (214), and (300) reflections of Fe_2O_3, as indicated by the JCPDS No. 86–2368 [43–46].

X-ray photon spectroscopy can ascertain oxidation states and other types of atom-to-atom bonding. Figure 2a illustrates the Ni 2p spectrum, which exhibits multiple discernible peaks. The identification of the $2p_{3/2}$ and $2p_{1/2}$ peaks, together with any satellite peaks, is accomplished by applying fitting procedures. The observed peaks at 853.6 eV are attributed to the Ni2p for nickel foam that supports the electrocatalyst [47–49]. Additionally, the peaks observed at 855, and 856 eV correspond to the presence of Ni^{2+} and Ni^{3+}, respectively. Furthermore, two peaks appear at binding energies of 872 and 875 eV, attributed to the $2p_{1/2}$ for Ni^{2+} and Ni^{3+}, respectively [50–52].

The spectrum of Co 2p exhibits two doublets resulting from spin–orbit coupling, together with two satellite peaks, as depicted in Figure 2b. The initial pair of peaks at 780.4 and 796.1 eV, and the subsequent pair at 782.1 and 798.3 eV, are identified as Co^{3+} and Co^{2+} ions, respectively. Two satellites at energy levels of 788.7 and 804.3 eV are equipped with the binding energy of Co^{3+} [53,54].

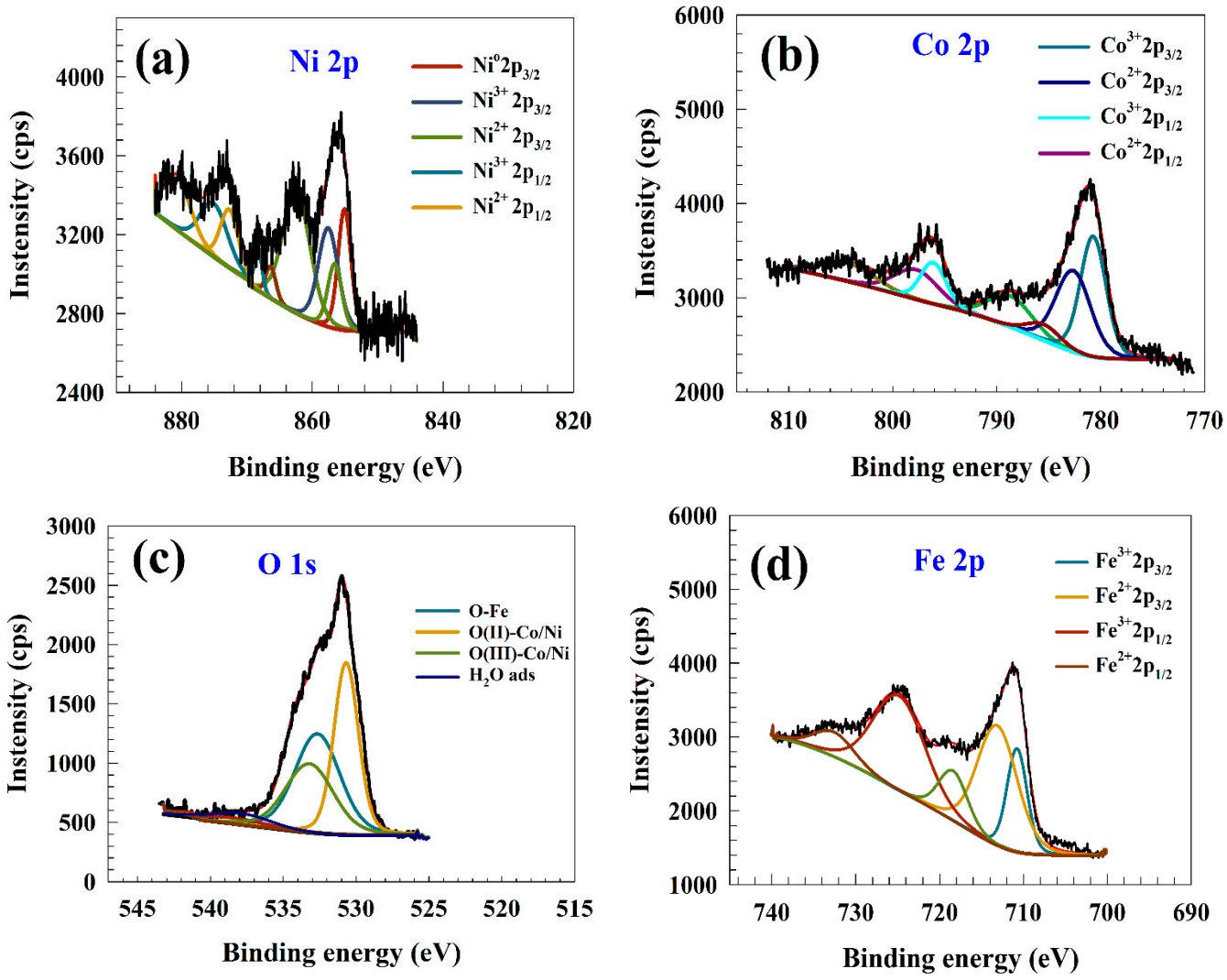

Figure 2. XPS spectrum of (**a**) Ni 2p, (**b**) Co 2P, (**c**) O1s, (**d**) Fe 2p.

Figure 2c shows the XPS results for the O1s core level. The observed peaks at a binding energy of 530.6 and 533.1 eV are associated with the metal–oxygen bond in $NiCo_2O_4$, specifically with the valence and lattice oxygen [55–59]. On the other hand, the peak observed at the binding energy of 532.5 eV is attributed to O-M in the Fe_2O_3 layer [60–62]. Otherwise, the observed peak at a binding energy of 536 eV can be attributed to the presence of gas-phase adsorbed water [63,64].

The obtained results further substantiated the presence of iron (Fe) on the nickel cobalt oxide/nickel foam ($NiCo_2O_4$/NF) composite material within the analyzed sample. Figure 2d displays the Fe 2p peaks. The two primary peaks observed at the 711.2 and 713.1 eV binding energies are attributed to the Fe (II) $2p_{3/2}$ and Fe (III) $2p_{3/2}$ states, respectively. The energy peak observed at 724 eV can be attributed to the Fe $2p_{1/2}$ electron transition, but the peak observed at 731 eV is associated with the satellite peak of the Fe $2p_{1/2}$ transition [65–67].

The morphological characteristics of the nickel foam and nanostructures of Fe@$NiCo_2O_4$ were analyzed using scanning electron microscopy (SEM), as depicted in Figure 3a–c. Figure 3a depicts the varying magnifications of the hollow structure observed in the nickel foam. Figure 3b displays the surface morphology of the Fe@$NiCo_2O_4$/NF material in its as-prepared state, as observed under a scanning electron microscope (SEM). The dimensions of the particles range from 40 to 95 nanometers. The reduced particle size of Fe@$NiCo_2O_4$ suggests an enhanced activity level in the resulting materials. Structural stability was

investigated using SEM; the SEM of the modified Fe@$NiCo_2O_4$/NF after the stability test is represented in Figure 3c. Some deterioration in particle shape was noticed due to being soaked in an alkaline medium for a long time.

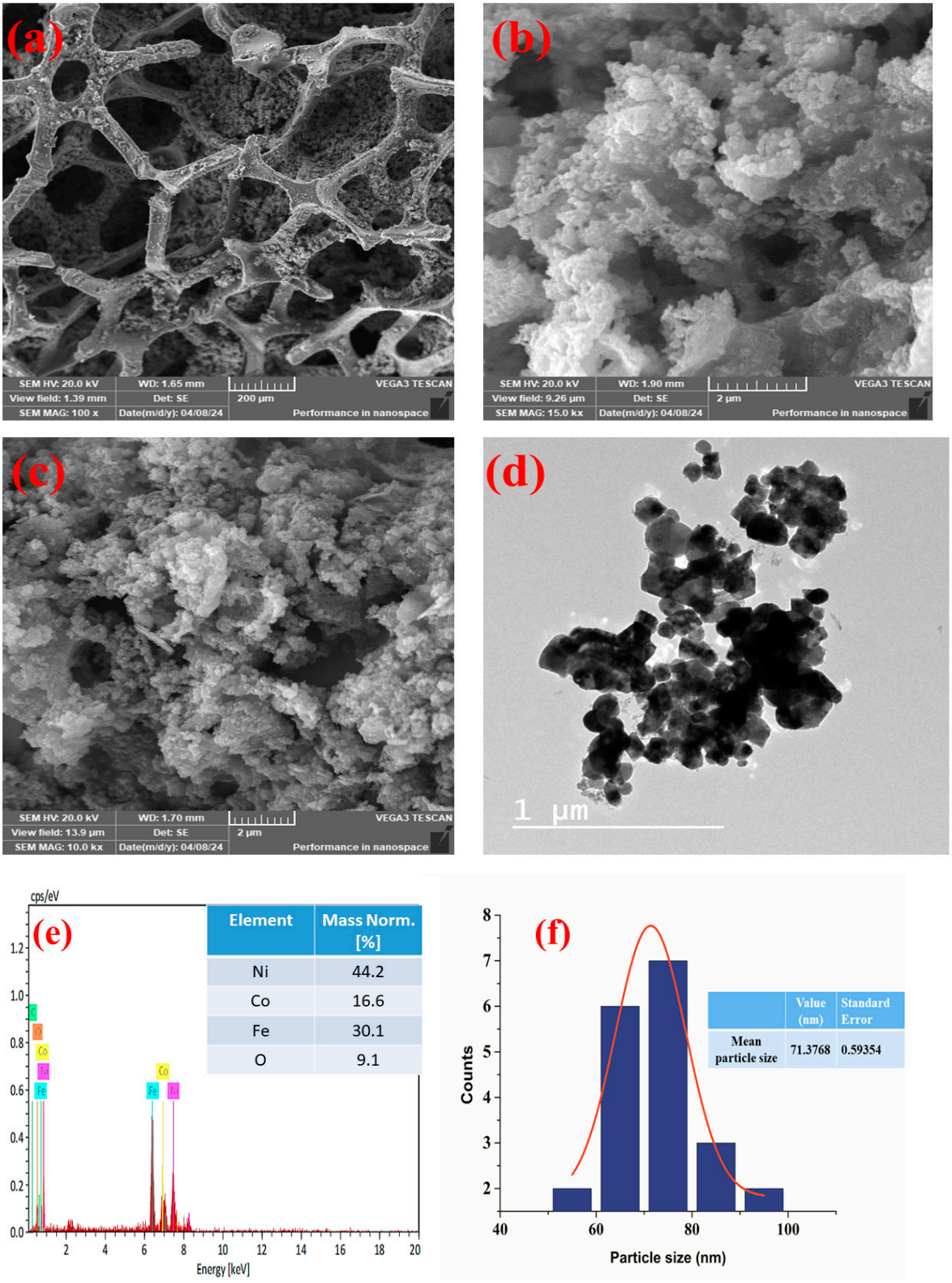

Figure 3. (**a**,**b**) SEM of Fe@$NiCo_2O_4$/NF, (**c**) SEM of Fe@$NiCo_2O_4$/NF after stability experiment, (**d**) TEM of Fe@$NiCo_2O_4$. (**e**) EDX of Fe@$NiCo_2O_4$/NF, (**f**) particle size distribution of Fe@$NiCo_2O_4$.

The conventional method employed for the determination of Fe@$NiCo_2O_4$ nanoparticle sizes involved the use of transmission electron microscopy (TEM). The average particle size of Fe@$NiCo_2O_4$ was measured to be 70 nanometers. The transmission electron microscopy (TEM) image of Fe@$NiCo_2O_4$ is depicted in Figure 3d.

Therefore, the energy-dispersive X-ray spectroscopy (EDX) analysis revealed the existence of nickel (Ni), cobalt (Co), iron (Fe), and oxygen (O) elements. Figure 3e illustrates the elemental composition of the Fe@$NiCo_2O_4$ sample. The elemental percentages depicted in the inset figure are the intended composition of Fe@$NiCo_2O_4$, whereas the high percentages of nickel depicted in EDX data are due to the Ni-foam, in addition to the higher iron percentage regarding the method for sample preparation by electrodeposition on $NiCo_2O_4$/NF. As represented in Figure 3f, the particle size distribution is established by the Gaussian fitting of TEM data.

In addition, an investigation was conducted to analyze the distribution of elements on the surface of Fe@$NiCo_2O_4$/NF through the utilization of elemental mapping techniques (refer to Figure 4). The anticipated materials can be confirmed by detecting the Ni, Co, Fe, and O elements. The great reactivity of the electrode towards the conversion of organic molecules can be elucidated by considering the loud distribution of metals on its surface.

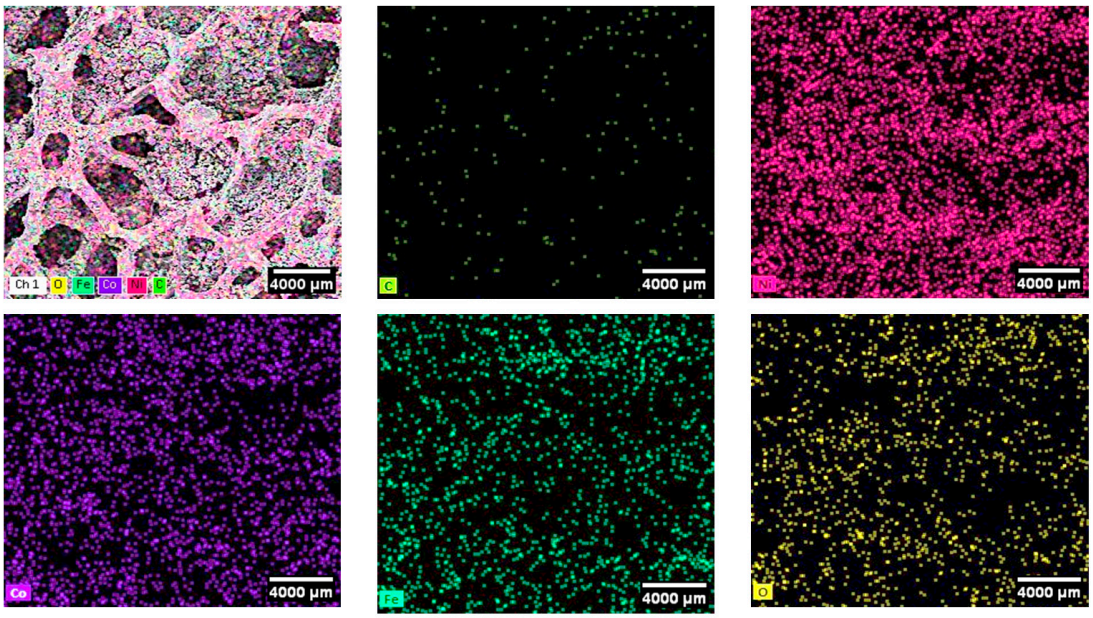

Figure 4. Surface mapping of Fe@$NiCo_2O_4$/NF. Surface of Fe@$NiCo_2O_4$/NF overall elements, C, Ni, Co, Fe, and O.

2.2. Electrochemical Activity Fe@$NiCo_2O_4$/NF

The modified Fe@$NiCo_2O_4$/NF activity was investigated in a 1.0 M NaOH solution using cyclic voltammetry. Given the significance of activating nickel-based electrodes in the electrochemical oxidation of small molecules, an initial approach was employed to enhance the performance of the electrodes by an activation strategy. The process led to the generation of NiOOH, a nickel-based compound that exhibits a significant degree of electrocatalytic efficacy. The activation step was conducted by employing repeated CVs in solution comprising a 1.0 M NaOH sweep rate of 200 mV s^{-1}. The occurrence of NiOOH generation during successive cycles is responsible for the increase in current. According to the data presented in Figure 5, the magnitude of the NiOOH layer's thickness exhibits a linear relationship with the number of potential sweeps. The acceleration of the conversion rate between $Ni(OH)_2$ and NiOOH can be ascribed to the existence of OH ions, as indicated by Equation (1) [68] as follows:

$$6\ Ni(OH)_2 + 6\ OH^- \leftrightarrow 6\ NiOOH + 6H_2O + 6e^- \quad (1)$$

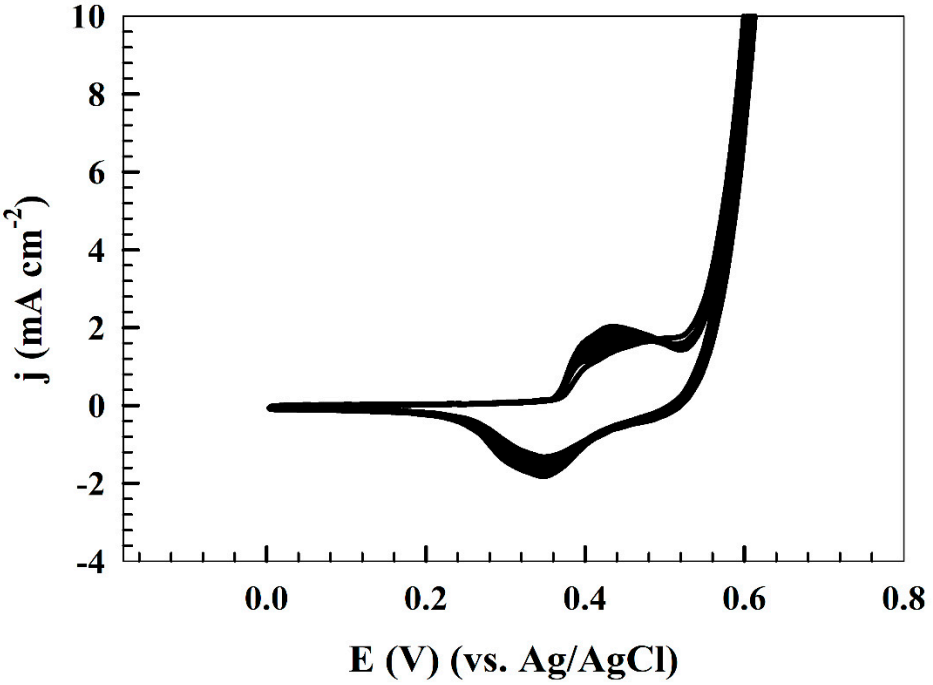

Figure 5. Repeated CVs of modified Fe@$NiCo_2O_4$/NF electrode in 1.0 M NaOH.

The utilization of nickel foam as a catalyst support has been extensively employed, resulting in improved electrocatalytic activity for the electro-oxidation of organic small molecules. Nevertheless, recent findings have revealed that the utilization of NF leads to an augmentation in the electrode surface's electrical conductivity and enhances the catalyst's durability. The presence of active NiOOH species greatly influences the conversion of ethylene glycol. The surface coverage was determined using Equation (2) in the absence of fuel. Various scan speeds ranging from 5 to 100 mV s^{-1} were employed, and the corresponding results are presented in Figure 6. The surface coverage can be estimated from the following equation:

$$Ip = (n^2 F^2/4RT)\ \nu\ A\ \Gamma \quad (2)$$

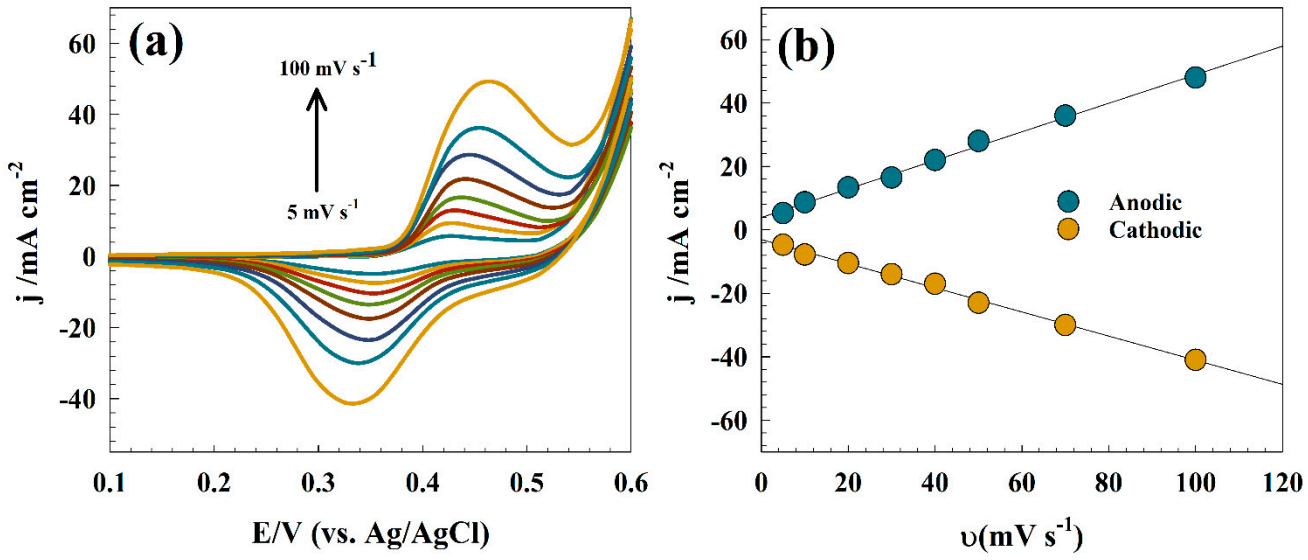

Figure 6. (**a**) CVs of Fe@$NiCo_2O_4$/NF in solution of 1.0 NaOH at various sweep rates, (**b**) linear relation between scan rate versus peak current densities.

Ip is the current of an anodic or cathodic peak, n is the number of electrons used, F is the Faraday constant, A is the electrode area, and Γ is the surface coverage.

Figure 6a shows the CV of modified Fe@$NiCo_2O_4$/NF in 1.0 M NaOH in the absence of organic molecules throughout a large scan range. The surface coverage was determined by a linear relationship between the oxidation current and scan rate (see Figure 6b). As a result, the surface coverage offered for the changed surface is 9.14×10^{-7} cm^2 s^{-1}.

2.2.1. Urea Electro-Oxidation

Urea demonstrates significant fuel properties due to its ability to be produced on a wide scale using the petrochemical process. Moreover, it is important to acknowledge that water with a substantial concentration of urea can be observed in the sludge generated from industrial operations, as well as in human urine detected in wastewater. Urea fuel cells (DUFCs) are now witnessing substantial expansion in fuel-cell technology. The electrochemical oxidation of urea is widely recognized as a six-electron process, which can be mathematically represented by Equation (3) [20].

$$H_2N\text{-}CO\text{-}NH_2 + 6OH^- \leftrightarrow N_2 + 5H_2O + CO_2 + 6\,e^- \quad (3)$$

Figure 7a displays the cyclic voltammogram (CV) of the modified $NiCo_2O_4$/NF and Fe@$NiCo_2O_4$/NF electrodes immersed in a solution containing 1.0 M urea and 1.0 M NaOH. Consequently, the electrochemical analysis reveals the presence of two distinct oxidation peaks occurring at a potential of approximately 0.58 V relative to the Ag/AgCl reference electrode. Furthermore, the reduction process reaches its maximum at a potential of 0.36 V (against Ag/AgCl), which can be attributed to the conversion of Ni(III) to Ni(II). Otherwise, the modified Fe@$NiCo_2O_4$/NF shows a higher current for urea oxidation compared to the unmodified $NiCo_2O_4$/NF. Thus, the peak position for urea oxidation shifts toward a more negative value by the addition of Fe_2O_3 layers.

In addition, the Tafel slope was determined to measure urea conversion through linear sweep voltammetry with a scan rate of 1 mV s^{-1}. The Tafel pattern of the modified $NiCo_2O_4$/NF and Fe@$NiCo_2O_4$/NF electrode is depicted in Figure 7b. The given Tafel slope is 104 and 85 mV dec^{-1} for $NiCo_2O_4$/NF and Fe@$NiCo_2O_4$/NF, respectively. Tafel graphs were generated for the electro-oxidation of urea using a modified electrode Fe@$NiCo_2O_4$/NF under quasi-steady-state polarization conditions. The experimental setup involved a solution of 1.0 M urea and 1.0 M NaOH. The logarithmic relationship between anodic current and overpotential can be observed in Figure 7b. The electrochemical sensitivity of the modified electrode Fe@$NiCo_2O_4$/NF toward variations in fuel concentration was also examined. In the experimental setup, a solution with a concentration of 1.0 M NaOH was utilized. The urea concentration in the solution varied within the range of 0.1 M to 1.0 M. The scan rate employed during the experiment was 20 mV s^{-1}, as depicted in Figure 7c. The findings of this study demonstrate that the suggested composite material has the potential for utilization in many applications, such as urea electro-oxidation in wastewater treatment, hydrogen production, and fuel cells, particularly in scenarios where the urea concentration varies. The urea concentration and the anodic peak current are related to each other and are depicted in Figure 7d.

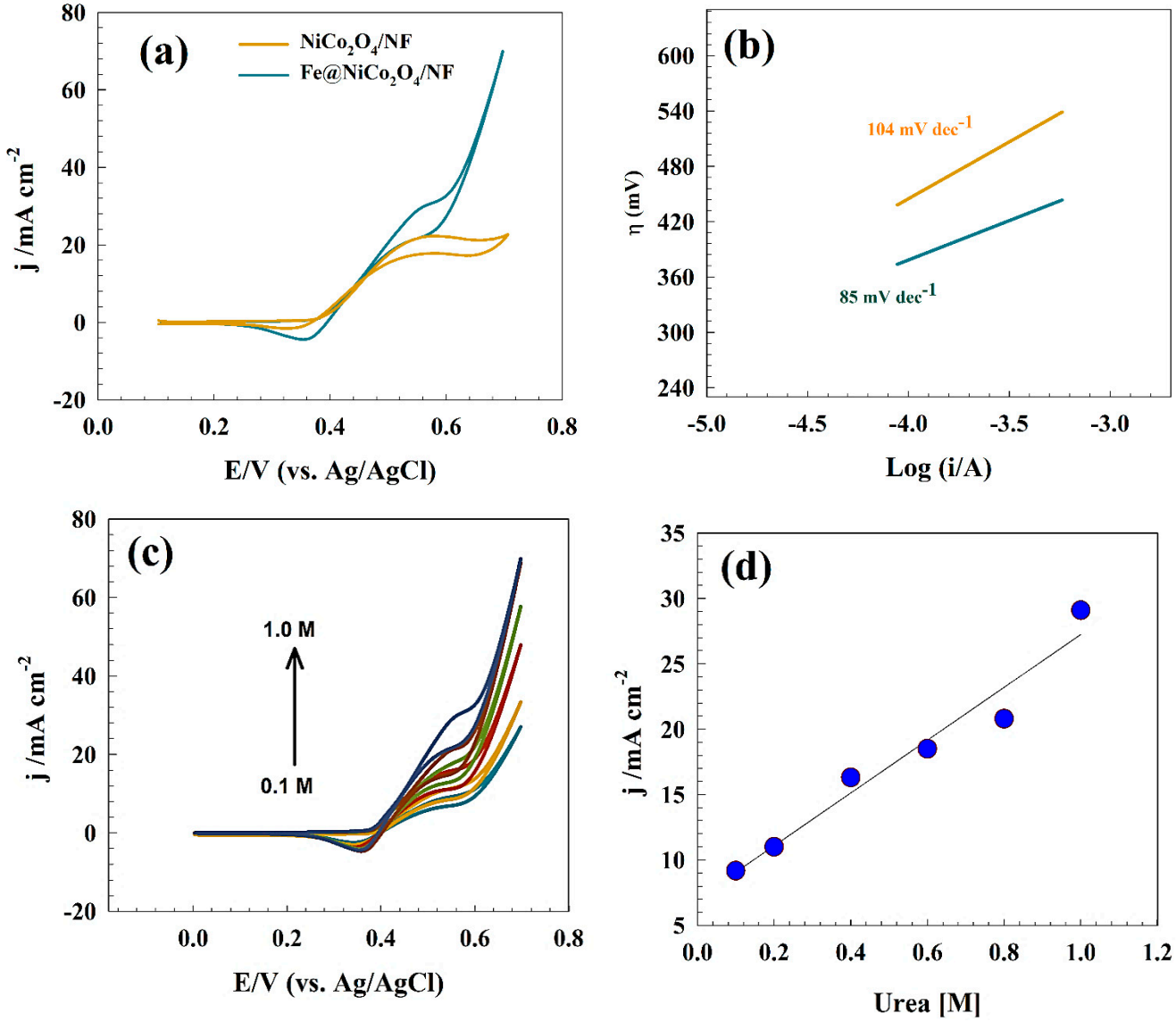

Figure 7. (**a**) CV of Fe@$NiCo_2O_4$/NF in alkaline and urea solution, (**b**) Tafel slope of urea oxidation, (**c**) CV of Fe@$NiCo_2O_4$/NF in different urea concentrations, (**d**) linear relation of anodic current versus urea concentrations.

2.2.2. Ethanol Electro-Oxidation

Ethanol is well recognized as a biodegradable and relatively non-toxic substance that is produced by the process of biomass fermentation or ethylene hydration, which involves the conversion of a petroleum component. Ethanol, an alcohol compound, is characterized by the presence of a carbon–carbon (C-C) bond and demonstrates a higher energy density in comparison to methanol. This phenomenon could be due to the molecule's capacity to release a total of twelve electrons during the process of complete oxidation to carbon dioxide, as illustrated by Equation (4) as follows:

$$CH_3CH_2OH + 12OH^- \leftrightarrow 2CO_2 + 9\,H_2O + 12e^- \quad (4)$$

Figure 8a displays the cyclic voltammogram (CV) of the $NiCo_2O_4$/NF and Fe@$NiCo_2O_4$/NF composite material in the presence of ethanol. Therefore, the oxidation peak detected at around 0.5 V (against Ag/AgCl) was ascribed to the conversion of ethanol. The observed displacement of the ethanol peak towards a more negative value concerning the urea peak can be attributed to the electrode's superior capacity for ethanol

oxidation compared to its performance with urea. Furthermore, the current density of the Fe@$NiCo_2O_4$/NF-modified electrode was observed to increase by ~35% compared with the unmodified $NiCo_2O_4$/NF surface.

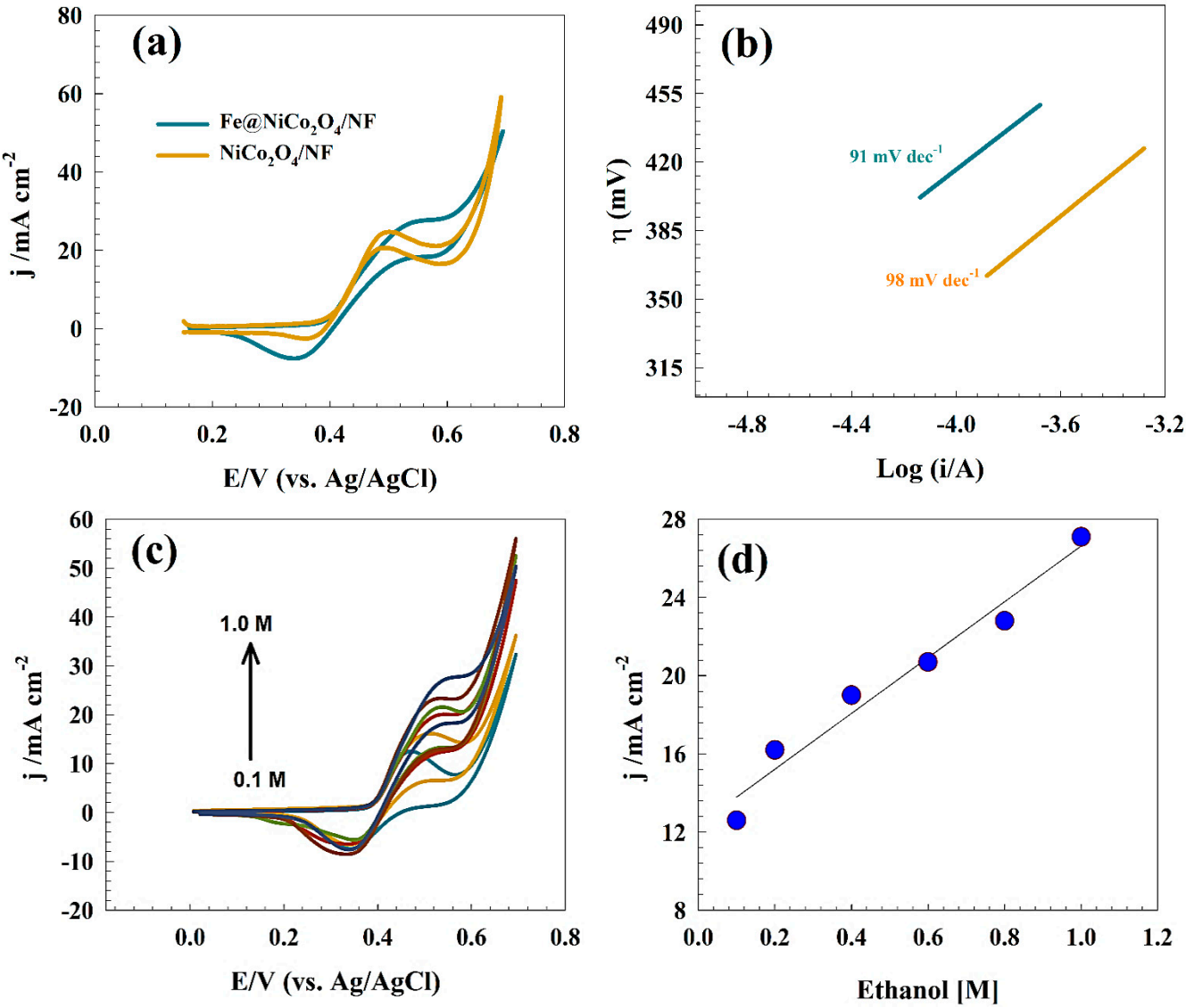

Figure 8. (**a**) CV of Fe@$NiCo_2O_4$/NF in alkaline and ethanol solution, (**b**) Tafel slope of ethanol oxidation, (**c**) CV of Fe@$NiCo_2O_4$/NF in different ethanol concentrations, (**d**) linear relation of anodic current versus ethanol concentrations.

Figure 8b illustrates a Tafel diagram representing the Fe@$NiCo_2O_4$/NF electrode employed for the oxygen evolution reaction. The Tafel slope of 98, 91 mV dec^{-1} has been determined for many modified surfaces of $NiCo_2O_4$/NF and Fe@$NiCo_2O_4$/NF, with the lower Tafel slope for Fe@$NiCo_2O_4$/NF compared to neat $NiCo_2O_4$/NF reflecting the higher activity of the iron-modified sample.

Fe@$NiCo_2O_4$/NF's Tafel slope for ethanol oxidation in an alkaline media was found to be equivalent to that of other modified surfaces, including Ni@NiO NWA/Pt (87 mV dec^{-1}) [69], and Ni-Pd nanoflower (164 mV dec^{-1}) [70].

Moreover, a study was undertaken to examine the electro-oxidation of ethanol across a range of concentrations, ranging from 0.1 M to 1.0 M. Based on the findings depicted in Figure 8c, it can be observed that no indications of surface saturation were detected within the investigated concentration range. Based on the data presented in Figure 8d, there is a

positive correlation seen between the anodic peak current of ethanol's electro-oxidation and the concentration of ethanol. The findings of this study indicate that the electrode under investigation exhibits favorable characteristics for implementation in diverse applications, including direct ethanol fuel cells (DEFCs).

2.2.3. Ethylene Glycol Electro-Oxidation

Ethylene glycol (EG), a cost-effective compound with a high boiling point, has attracted considerable interest. Furthermore, it is essential to highlight that EG's energy capacity, roughly 4.8 A h mL^{-1}, exceeds that of methanol, which is 4 A h mL^{-1} [16]. Based on the structural composition of ethylene glycol (EG), the conversion process from ethylene glycol to carbon dioxide (CO_2) necessitates the utilization of 10 electrons per alcohol molecule. The reaction under consideration can be mathematically expressed as Equation (5) as follows:

$$HO\text{-}CH_2\text{-}CH_2\text{-}OH + 2H_2O \leftrightarrow 2CO_2 + 5H_2 + 10\,e^- \quad (5)$$

Figure 9a represents CV that indicates the activity of $NiCo_2O_4$/NF and Fe@$NiCo_2O_4$/NF electrodes toward ethylene glycol electro-oxidations. The undefined peak observed for ethylene glycol is with regard to different possible molecules that ethylene glycol could oxidize, like glycolaldehyde, glyoxal, glycolic acid, and glyoxylic acid [24]. The addition of Fe_2O_3 to the $NiCo_2O_4$ spinel oxide led to enhanced activity toward EG electro-oxidation, whereas Fe_2O_3 could enhance the charge transfer process due to the high electrical conductivity of iron-based materials compared to $NiCo_2O_4$.

A Tafel diagram of the $NiCo_2O_4$/NF and Fe@$NiCo_2O_4$/NF electrodes for the oxygen evolution reaction is shown in Figure 9b. The Tafel slope for Fe@$NiCo_2O_4$/NF has been calculated as 130 and 120 mV dec^{-1} for $NiCo_2O_4$/NF and Fe@$NiCo_2O_4$/NF, respectively. By comparison, the Fe@$NiCo_2O_4$/NF Tafel slope was discovered to be comparable to those of other modified surfaces for ethylene glycol oxidation in an alkaline medium, such as NiCo @chitosan (88 mV dec^{-1}) [24], IN738 supper alloy (80 mV dec^{-1}) [68], and PtPdAuCuFe/C (80 mV dec^{-1}) [71].

The efficacy of the electrode in eliminating ethylene glycol was assessed by measuring the activity of each electrode throughout a wide range of ethylene glycol concentrations. Figure 9c exhibits the cyclic voltammograms (CVs) of Fe@$NiCo_2O_4$/NF-modified electrodes in a 1.0 M NaOH solution, with a scan rate of 20 mV s^{-1}. A significant increase in the anodic peak current was seen across a wide range of ethylene glycol concentrations. The oxidation reaction of ethylene glycol on the electrode exhibited a diffusion limitation, as seen by the slight change in peak potential with respect to concentration. Hence, the augmentation of ethylene glycol concentrations exerted an influence on the diffusion of ethylene glycol toward the surface of the electrode. The graphical depiction in Figure 9d demonstrates the linear correlation between the concentration of ethylene glycol and the anodic peak current, specifically at a potential of 0.6 V (vs. Ag/AgCl). This representation highlights the significant efficacy of the electro-oxidation process for ethylene glycol, as it prevents the electrode from reaching surface saturation, even when exposed to high concentrations such as 1.0 M ethylene glycol.

The electrochemical oxidation upon Fe@$NiCo_2O_4$/NF surfaces for urea, ethanol, and ethylene glycol was compared with others reported in the literature (see Table 1).

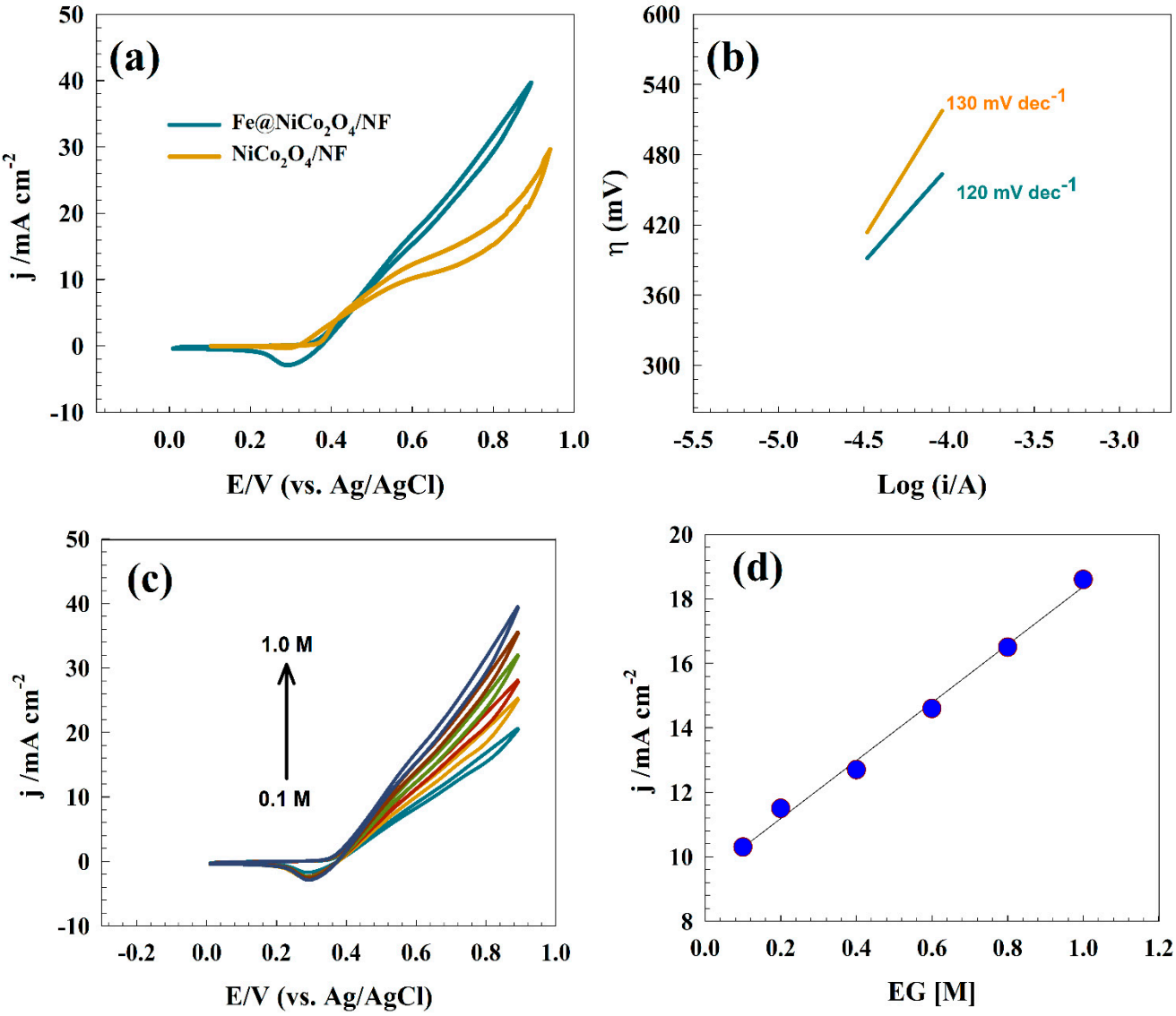

Figure 9. (**a**) CV of Fe@$NiCo_2O_4$/NF in alkaline and ethylene glycol solutions, (**b**) Tafel slope of ethylene glycol oxidation, (**c**) CV of Fe@$NiCo_2O_4$/NF in different ethylene glycol concentrations, (**d**) linear relation of anodic current versus ethylene glycol concentrations.

Table 1. Comparison between the results of Fe@$NiCo_2O_4$/NF and others reported in the literature.

Anode Material	Fuel	Electrolyte Concentration (mol L^{-1})	Fuel Concentration (mol L^{-1})	Sweep Rate (mV s^{-1})	I_p (mA cm^{-2})	Tafel Slope (mV/dec)	Ep (V)	Reference
Fe@$NiCo_2O_4$/NF	Urea	1.0	1.0	20	31	85	0.55 (vs. Ag/AgCl)	This work
Fe@$NiCo_2O_4$/NF	Ethanol	1.0	1.0	20	27	91	0.55 (vs. Ag/AgCl)	This work
Fe@$NiCo_2O_4$/NF	Ethylene glycol	1.0	1.0	20	17	120	0.58 (vs. Ag/AgCl)	This work
Cu@NiO/GC	Urea	0.5	0.3	20	32	48	0.58 (vs. Ag/AgCl)	[72]
NiO@MnOx/Pani/Gr	Urea	1.0	0.3	50	20	73	0.5 (vs. Ag/AgCl)	[73]
IN738 supper alloy	Ethanol	1.0	1.0	20	29	52	0.55 (vs. Ag/AgCl)	[68]
Pt/C	Ethanol	1.0	1.0	50	4.9	132	−0.1 (vs. Hg/HgO)	[74]
Pt–MgO	Ethanol	1.0	1.0	50	27.1	129	−0.2 (vs. Hg/HgO)	[74]
PdNiP/C	Ethylene glycol	1.0	1.0	20	31	-	−0.3 (vs. SCE)	[75]
PdNi/Sulfonate-MWCNT	Ethylene glycol	0.5	1.0	50	35	-	0.2 (vs. Ag/AgCl)	[76]
$NiCo_2O_4$@Chitosan	Ethylene glycol	1.0	1.0	20	42	88	0.48 (vs. Ag/AgCl)	[24]
Mo-doped PtBi	Ethylene glycol	1.0	1.0	50	61.1	113	−0.1 (vs. Ag/AgCl)	[77]

2.3. Effect of Scan Rate and Surface Durability

Furthermore, certain kinetic parameters, such as the diffusion coefficient, were computed. Figure 10a,b depict the visual representations. This study examines the influence of varying the scan rate within the range of 5 to 1000 mV s^{-1} on the electrochemical characteristics of the Fe@$NiCo_2O_4$/NF electrode in a 1.0 M fuel solution composed of urea and ethanol, in conjunction with a 1.0 M NaOH electrolyte. Using the Randles–Sevcik equation (Equation (6)), the diffusion coefficient was determined by establishing the link between the square root of scan rates and anodic peak currents.

$$I_p = 2.99 \times 10^5 \, n \, A \, C_o \, [(1 - \alpha) \, n_o \, D \, v]^{0.5} \quad (6)$$

where I_p is the anodic peak, n is the electron number (n = 6 for urea, n = 12 for ethanol, and n = 10 for ethylene glycol), Co is the initial concentration of fuels, D is the diffusion coefficient, v is the scan rate, and A is the electrode area. The estimation of the diffusion coefficient is determined using the linear correlation seen between the anodic current and the square root of the sweep rate, as depicted in Figure 10c. The diffusion coefficients for urea and ethanol in modified Fe@$NiCo_2O_4$/NF are reported as 4.6×10^{-6} and 2.6×10^{-6} cm^2 s^{-1}, respectively. The elevated diffusion coefficient of urea can be attributed to its diminutive molecular size and reduced intermolecular interactions.

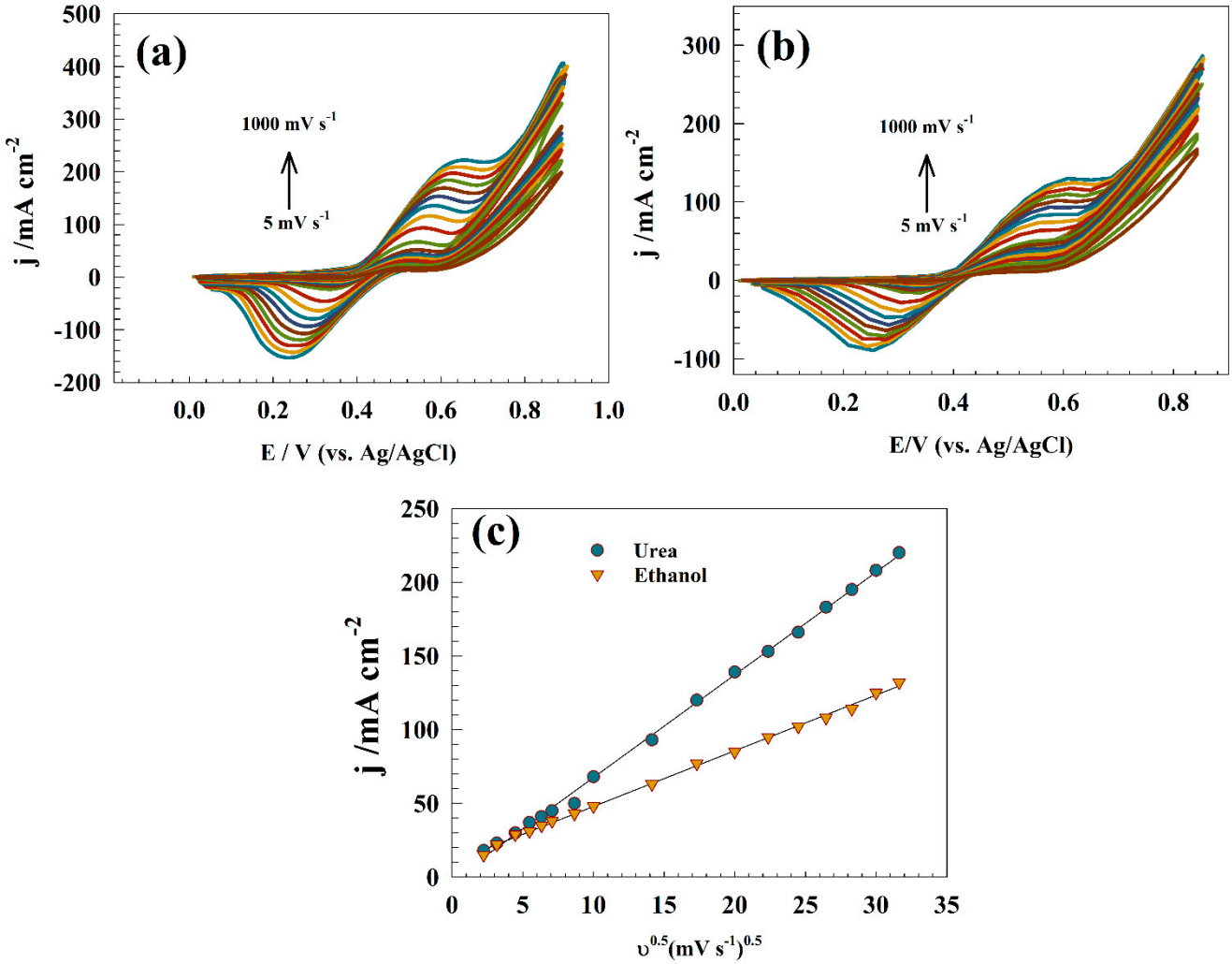

Figure 10. (**a**,**b**) CVs of Fe@$NiCo_2O_4$/NF in the solution of 1.0 M fuel (urea and ethanol) at wide ranges of scan rates. (**c**) Linear relation between anodic current versus square root of scan rate.

The examination of the electrode's durability is regarded as a crucial aspect. The technique of chronoamperometry with a constant potential was employed to investigate the stability of the electrode. The chronoamperograms of the different modified surfaces were observed for 300 min at a consistent potential of 0.6 V (vs. Ag/AgCl) in a solution containing 1.0 M NaOH and 1.0 M of urea, ethanol, and ethylene glycol, as depicted in Figure 11, which shows a chronoamperogram of the Fe@$NiCo_2O_4$/NF electrode. Consequently, urea, ethanol, and ethylene glycol activity exhibited a respective decrease of 17.8%, 20.3%, and 31%. The projected durability of the electrode can be related to its ability to withstand carbon monoxide, which is facilitated by the inclusion of many transition metals in its crystal structure. Therefore, the Fe@$NiCo_2O_4$/NF structure possesses inherent stability, which substantially reduces the loss of catalyst mass. The decrease in electrical current can be ascribed to multiple processes, such as surface poisoning, electrode surface degradation, and incompletely oxidized species [78–80]. The presence of a co-catalyst affects the expected carbon monoxide (CO) tolerance of Fe@$NiCo_2O_4$/NF. The resistance of CO adsorption by Ni-based co-catalysts has been noted in previous studies [81].

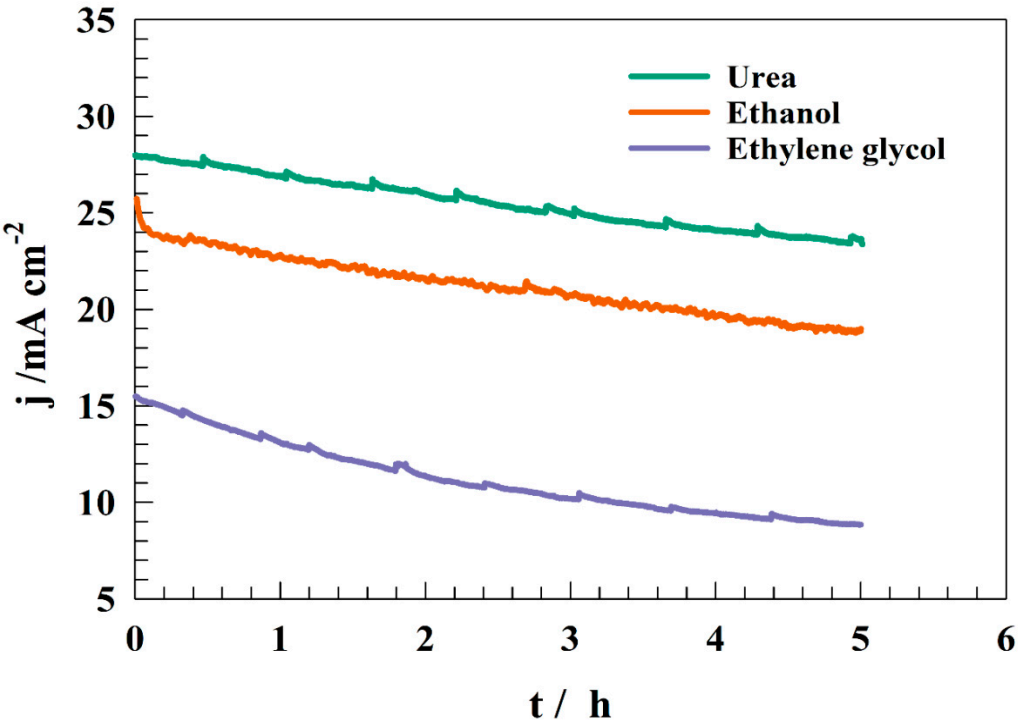

Figure 11. Chronoamerogram of Fe@$NiCo_2O_4$/NF with various fuels (urea, ethanol, and ethylene glycol).

Furthermore, electrochemical impedance spectroscopy is a powerful technique used to study the electrical properties of materials, such as ionic conductivity and charge transfer resistance. It involves applying a small-amplitude AC signal to a material and measuring the resulting impedance response over a range of frequencies. This method is commonly used in the field of electrochemistry to analyze the behavior of electrodes in various electrochemical systems. For example, researchers may use electrochemical impedance spectroscopy to study the performance of fuel cells by measuring the impedance of the electrode–electrolyte interface. By analyzing the impedance data, they can gain insights into the kinetics of electrochemical oxidation and charge transfer processes.

However, the performance of the modified Fe@$NiCo_2O_4$/NF was investigated toward different fuel oxidations using the EIS technique. The Nyquist plot of Fe@$NiCo_2O_4$/NF at a solution of 1.0 M fuel at a constant potential of 0.6 V is shown in Figure 12. Thus, the EIS data were fitted using NOVA software (version 2.1), while, the data were explained using two equivalent circuits (see Figure 12 inset). the Nyquist data showed that the urea

electro-oxidation is a pure charge transfer process (Circuit no. 1). On the other hand, the electro-oxidation of ethanol and ethylene glycol exhibits some diffusion properties along with the charge transfer process (Circuit no. 2). However, as the equivalent circuit for the electrochemical impedance research, a comparable electric circuit was used. Resistance to the solution (Rs), resistance of the outer layer (R_1), and resistance of the inner layer of the surface (R_2) were determined. In addition, the two capacitors were enrolled in equivalent circuits, like C_1, which represents double-layer capacitance, and C_2, which represents the capacitance of the inner layer of the electrode surface. Furthermore, the diffusion parameter (W) reflects the presence of a diffusion-controlled region in circuit no. 2.

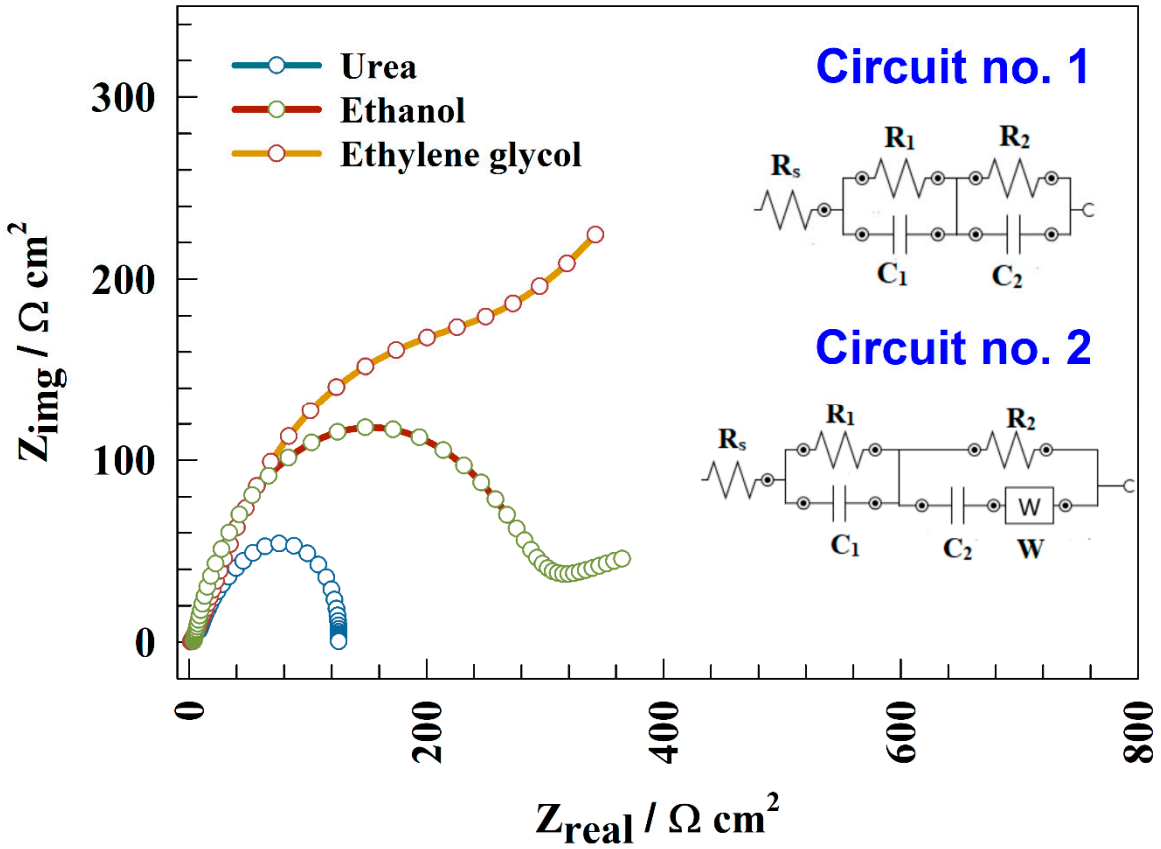

Figure 12. Nyquist plot of the Fe@$NiCo_2O_4$/NF electrode in the presence of different fuels.

According to fitted data, the oxidation of urea upon a modified electrode is a pure charge transfer process. On the other hand, the electrochemical oxidation of both ethanol and ethylene glycol is considered as a mixture of the charge transfer and diffusion processes. Furthermore, the presence of two charge transfer circuits indicates that the oxidation of fuel on Fe@$NiCo_2O_4$/NF takes place through two different layers (inner and outer).

Charge transfer resistance can be employed for determining the efficiency of the electrode toward the oxidation process. As listed in Table 2, the electrode exhibited lower charge transfer resistance for urea compared to ethanol and ethylene glycol, which can be confirmed by data obtained by the CV technique.

Table 2. Representation of fitting parameters for modified Fe@$NiCo_2O_4$/NF in the presence of different fuels.

Fuel	R_s (Ω cm^2)	R_1 (Ω cm^2)	R_2 (Ω cm^2)	C_1 (F)	C_2 (F)	W (Ω $s^{-1/2}$)
Urea	3	16	117	0.00182	0.002471	-
Ethanol	6	21	360	0.00161	0.002198	0.001756
Ethylene glycol	5	26	410	0.00117	0.002071	0.001019

3. Experimental Section

3.1. Instruments and Devices

The Fe@NiCo2O4/NF samples were analyzed using X-ray diffraction (XRD) with Cu-Kα radiation (λ = 1.5406 Å) on an Analytical X'Pert instrument to determine their structures. The electrocatalyst with the highest activity for urea oxidation was analyzed using X-ray photoelectron spectroscopy (XPS). The analysis was conducted using a K-ALPHA instrument (Thermo Fisher Scientific, Inc., Waltham, MA, USA) with monochromatic X-ray Al K-alpha radiation ranging from 10 to 1350 eV. The spot size was 400 m, and the pressure was maintained at 10^{-9} mbar. The total spectrum pass energy was set at 200 eV, while the narrow spectrum pass energy was set at 50 eV. XPS was fitted using Casa XPS software (version 2.3.26). The Tescan SEM (TESCAN VEGA 3, Brno, Czech Republic) was utilized to examine the scanning electron microscope. The samples were affixed onto aluminum stubs using sticky carbon tape and subsequently coated with a layer of gold (Au) for a duration of 150 s using the Quorum techniques Ltd., East Sussex, UK) sputter coater (Q150t, Sussex, England). The surface morphology was assessed using high-resolution transmission electron microscopy (HR-TEM) with a JEOL JEM-2100 instrument from JEOL, Tokyo, Japan.

3.2. Synthesis of Fe@$NiCo_2O_4$/NF

Nickel foam (NF) samples with dimensions of 0.5 cm × 0.5 cm were submerged in a flask containing 15 mL of a diluted hydrochloric acid (HCl) solution with a concentration of 1.0 M to remove surface oxides and impurities. The flask was then put inside an ultrasonic bath that was programmed to run for 25 min at a power level of 100 W and a frequency of 80 kHz while keeping the temperature in the area at ambient. After being placed in a flask with deionized (DI) water, the NF samples were subjected to ultrasonication for 10 min. Any remaining oxides that might have been present on the sample surfaces were completely removed using the technique. The samples were then moved to a solution made of 100% ethanol, and they underwent an additional 10 min of ultrasonication [82].

In this experimental setting, a solution comprising $Co(NO_3)_2.6H_2O$ and $Ni(NO_3)_2.6H_2O$ was created. The recommended molar ratio for nickel to cobalt is 1:2. The solute was dissolved in a solution of deionized (DI) water and absolute ethanol in a 1:1 proportion. The resultant solution was thereafter subjected to vigorous stirring for a duration of 30 min utilizing a magnetic stirrer operating at ambient temperature. Following that, a solution containing 10 mM of NH_4F and 18 mM of urea was put into the vessel. The mixture was then agitated for an additional length of 30 min. Throughout the duration of this process, the container maintained a securely sealed state. The complete solution was meticulously put into a 60 mL autoclave made of stainless steel and covered with Teflon. The autoclave contained a vertically oriented pre-treated nickel foam (NF) substrate, which served as the base for the subsequent $NiCo_2O_4$/NF sample fabrication. The autoclave was maintained in a tightly sealed and undisturbed state for a duration of 20 h, during which, a hydrothermal reaction took place at a temperature of 160 degrees Celsius. Following this, the autoclave was removed from the furnace and left to cool down at the surrounding room temperature. The gel-like substance formed was treated to a series of washes using deionized water and absolute ethanol in order to eliminate any residual reactants and undesirable byproducts. Following that, the product was dried in an oven set at a temperature of 60 °C for 24 h.

Following this, the process of air calcination was carried out by exposing the dehydrated materials to a furnace operating at a temperature of 400 °C for 3 h. Subsequently, iron was electrochemically deposited onto the $NiCo_2O_4$/NF substrate using a solution containing 0.1 M $FeSO_4$, 0.4 M H_3PO_4, and 0.5 M Na_2SO_4. The cyclic voltammetry technique was utilized to facilitate the electrochemical deposition of iron. This involved the application of 50 cyclic voltammograms (CVs) at a scan rate of 50 mV s^{-1} within a potential range of 0.2 to −1.2 V, relative to the Ag/AgCl reference electrode [83,84]. Finally, the Fe@$NiCo_2O_4$/NF composite was subjected to thorough rinsing with deionized water and subsequently subjected to a drying process in an oven set at a temperature of 60 °C for electrochemical analysis.

3.3. Electrochemical System

A nickel foam sample that underwent modifications was subjected to an experimental investigation to examine its electrochemical characteristics. The specimen's measurements were measured as 0.5 cm in length, 0.5 cm in width, and 2 mm in height. To assess the efficacy of the Fe@$NiCo_2O_4$/NF electrode in enhancing the electro-oxidation of urea, ethanol, and ethylene glycol (EG), a series of electrochemical studies were conducted. These experiments included cyclic voltammograms, chronoamperometry, and electrochemical impedance spectroscopy. The experimental setup consisted of a three-electrode device using a 1.0 M NaOH aqueous electrolyte. The experiment employed a platinum wire as the counter electrode and a KCl-saturated Ag/AgCl electrode as the reference electrode. The electrodes were employed to measure the required tests. The AUTOLAB workstation (PGSTAT128N) was utilized to conduct a variety of electrochemical experiments, such as cyclic voltammetry, chronoamperometry, and electrochemical impedance. The graphical user interface was developed using Nova software (version 2.1), namely version 2.1. Furthermore, a Tafel slope was detected using linear sweep voltammetry. The LSV was performed at a sweep rate of 1 mV s^{-1} in a solution of 1.0 M fuel (i.e., urea, ethyl alcohol, and ethylene glycol). Additionally, the potential window was selected to include all redox peaks for fuel conversions. The current was standardized by utilizing the electroactive surface area. The calculation of current density is contingent upon the actual surface area available for the electrochemical process. Thus, we employed the following correlation to estimate the electrochemically active surface area:

$$ESA = Q/sL$$

where Q is the amount of charge consumed to reduce the NiOOH to $Ni(OH)_2$, "s" is a constant that represents the monolayer of $Ni(OH)_2$ equal 257 μC cm^{-2}, and 'L' is the electrocatalyst loading 3.8×10^{-3} g cm^{-2}.

The charges were calculated by integrating the area under the curve for the reduction peaks in Figure 5 (using origin software (version 9)). Therefore, the ESA values are 32.1 m^2 g^{-1} for the Fe@ $NiCo_2O_4$/NF electrode.

4. Conclusions

The synthesis of nickel cobalt oxide on nickel foam was effectively achieved through the utilization of a hydrothermal method. The process of electrodeposition was employed to deposit iron onto the surface, utilizing cyclic voltammetry. The chemical structure of the anode that was created was confirmed by the utilization of X-ray photoelectron spectroscopy (XPS) research. The electrode exhibited significant reactivity towards the electrochemical oxidation of urea, ethanol, and ethylene glycol. The diminished reactivity of ethylene glycol can be attributed to the increased strength of intermolecular interactions between ethylene glycol and the surrounding solution. The unassigned peak observed during the oxidation of ethylene glycol can be attributed to a range of potential oxidation byproducts. The observation of a large resultant current during urea oxidation can be attributed to the easily accessible oxidation mechanism and the high diffusion coefficient of urea towards the electrode surface. The electrode exhibited a notable level of resilience

when exposed to tiny organic compounds. Consequently, no alterations in the electric current were detected during a period of 5 h of oxidation.

Author Contributions: Conceptualization, S.S.M., H.A.A. and M.A.H.; methodology, S.S.M. and M.A.H.; software, S.S.M. and M.A.H.; validation, S.S.M., N.S.A.-K., H.A.A. and M.A.H.; formal analysis, S.S.M., H.A.A., A.M.M., W.F.Z. and M.A.H.; investigation, S.S.M. and M.A.H.; resources, F.S.A., S.S.M., N.S.A.-K. and A.M.M.; data curation, S.S.M., W.F.Z. and M.A.H.; writing—original draft, F.S.A., S.S.M., A.M.M. and M.A.H.; writing—review and editing, S.S.M. and M.A.H.; visualization, N.S.A.-K. and W.F.Z.; supervision, F.S.A., N.S.A.-K., W.F.Z. and H.A.A.; project administration, F.S.A., N.S.A.-K., A.M.M. and H.A.A.; funding acquisition, F.S.A., N.S.A.-K., A.M.M., W.F.Z. and H.A.A. All authors have read and agreed to the published version of the manuscript.

Funding: This research was funded by "Princess Nourah bint Abdulrahman University Researchers Supporting Project number (PNURSP2024R107), Princess Nourah bint Abdulrahman University, Riyadh, Saudi Arabia".

Data Availability Statement: Data are contained within the article.

Acknowledgments: The authors extend their sincere appreciation to "Princess Nourah bint Abdulrahman University Researchers Supporting Project number (PNURSP2024R107), Princess Nourah bint Abdulrahman University, Riyadh, Saudi Arabia". The authors are thankful to the Deanship of Graduate Studies and Scientific Research at University of Bisha for supporting this work through the Fast-Track Research Support Program.

Conflicts of Interest: The authors declare that they have no known competing financial interests or personal relationships that could have appeared to influence the work reported in this paper.

References

1. Talebian-Kiakalaieh, A.; Amin, N.A.S.; Hezaveh, H. Glycerol for renewable acrolein production by catalytic dehydration. *Renew. Sustain. Energy Rev.* **2014**, *40*, 28–59. [CrossRef]
2. Talebian-Kiakalaieh, A.; Amin, N.A.S.; Najaafi, N.; Tarighi, S. A review on the catalytic acetalization of bio-renewable glycerol to fuel additives. *Front. Chem.* **2018**, *6*, 573. [CrossRef] [PubMed]
3. Höök, M.; Tang, X. Depletion of fossil fuels and anthropogenic climate change—A review. *Energy Policy* **2013**, *52*, 797–809. [CrossRef]
4. Perera, F.; Nadeau, K. Climate change, fossil-fuel pollution, and children's health. *N. Engl. J. Med.* **2022**, *386*, 2303–2314. [CrossRef] [PubMed]
5. Carrette, L.; Friedrich, K.A.; Stimming, U. Fuel cells: Principles, types, fuels, and applications. *ChemPhysChem* **2000**, *1*, 162–193. [CrossRef]
6. Lucia, U. Overview on fuel cells. *Renew. Sustain. Energy Rev.* **2014**, *30*, 164–169. [CrossRef]
7. Kordesch, K.; Simader, G. *Fuel Cells and Their Applications*; Wiley-VCH: Weinheim, Germany, 1996.
8. Cui, G.; Song, S.; Shen, P.K.; Kowal, A.; Bianchini, C. First-principles considerations on catalytic activity of Pd toward ethanol oxidation. *J. Phys. Chem. C* **2009**, *113*, 15639–15642. [CrossRef]
9. Song, H.M.; Anjum, D.H.; Sougrat, R.; Hedhili, M.N.; Khashab, N.M. Hollow Au@Pd and Au@Pt core–shell nanoparticles as electrocatalysts for ethanol oxidation reactions. *J. Mater. Chem.* **2012**, *22*, 25003–25010. [CrossRef]
10. Urbańczyk, E.; Jaroń, A.; Simka, W. Electrocatalytic oxidation of urea on a sintered Ni–Pt electrode. *J. Appl. Electrochem.* **2017**, *47*, 133–138. [CrossRef]
11. Hefnawy, M.A.; Nafady, A.; Mohamed, S.K.; Medany, S.S. Facile green synthesis of Ag/carbon nanotubes composite for efficient water splitting applications. *Synth. Met.* **2023**, *294*, 117310. [CrossRef]
12. Hefnawy, M.A.; Fadlallah, S.A.; El-Sherif, R.M.; Medany, S.S. Competition between enzymatic and non-enzymatic electrochemical determination of cholesterol. *J. Electroanal. Chem.* **2023**, *930*, 117169. [CrossRef]
13. Al-Kadhi, N.S.; Hefnawy, M.A.; Nafee, S.S.; Alamro, F.S.; Pashameah, R.A.; Ahmed, H.A.; Medany, S.S. Zinc Nanocomposite Supported Chitosan for Nitrite Sensing and Hydrogen Evolution Applications. *Polymers* **2023**, *15*, 2357. [CrossRef]
14. Galal, A.; Atta, N.F.; Hefnawy, M.A. Lanthanum nickel oxide nano-perovskite decorated carbon nanotubes/poly (aniline) composite for effective electrochemical oxidation of urea. *J. Electroanal. Chem.* **2020**, *862*, 114009. [CrossRef]
15. Li, N.; Sun, L.; Li, Q.; Xia, T.; Huo, L.; Zhao, H. Electrode properties of $CuBi_2O_4$ spinel oxide as a new and potential cathode material for solid oxide fuel cells. *J. Power Sources* **2021**, *511*, 230447. [CrossRef]
16. Lewis, M.J.; Zhu, J.H. A Process to Synthesize $(Mn, Co)_3O_4$ Spinel Coatings for Protecting SOFC Interconnect Alloys. *Electrochem. Solid State Lett.* **2011**, *14*, B9. [CrossRef]
17. Zhang, Q.; Martin, B.E.; Petric, A. Solid oxide fuel cell composite cathodes prepared by infiltration of copper manganese spinel into porous yttria stabilized zirconia. *J. Mater. Chem.* **2008**, *18*, 4341–4346. [CrossRef]

18. Galal, A.; Atta, N.F.; Hefnawy, M.A. Voltammetry study of electrocatalytic activity of lanthanum nickel perovskite nanoclusters-based composite catalyst for effective oxidation of urea in alkaline medium. *Synth. Met.* **2020**, *266*, 116372. [CrossRef]
19. Atta, N.F.; El-Sherif, R.M.A.; Hassan, H.K.; Hefnawy, M.A.; Galal, A. Conducting Polymer-Mixed Oxide Composite Electrocatalyst for Enhanced Urea Oxidation. *J. Electrochem. Soc.* **2018**, *165*, J3310–J3317. [CrossRef]
20. Zhang, T.; Yang, K.; Wang, C.; Li, S.; Zhang, Q.; Chang, X.; Li, J.; Li, S.; Jia, S.; Wang, J. Nanometric Ni_5P_4 clusters nested on $NiCo_2O_4$ for efficient hydrogen production via alkaline water electrolysis. *Adv. Energy Mater.* **2018**, *8*, 1801690. [CrossRef]
21. Cheng, J.P.; Wang, W.D.; Wang, X.C.; Liu, F. Recent research of core–shell structured composites with $NiCo_2O_4$ as scaffolds for electrochemical capacitors. *Chem. Eng. J.* **2020**, *393*, 124747. [CrossRef]
22. Liu, X.Y.; Zhang, Y.Q.; Xia, X.H.; Shi, S.J.; Lu, Y.; Wang, X.L.; Gu, C.D.; Tu, J.P. Self-assembled porous $NiCo_2O_4$ hetero-structure array for electrochemical capacitor. *J. Power Sources* **2013**, *239*, 157–163. [CrossRef]
23. Ding, Q.; Zou, X.; Ke, J.; Dong, Y.; Cui, Y.; Lu, G.; Ma, H. S-scheme 3D/2D NiCo2O4@ g-C3N4 hybridized system for boosting hydrogen production from water splitting. *Renew. Energy* **2023**, *203*, 677–685. [CrossRef]
24. Medany, S.S.; Hefnawy, M.A. Nickel–cobalt oxide decorated Chitosan electrocatalyst for ethylene glycol oxidation. *Surf. Interfaces* **2023**, *40*, 103077. [CrossRef]
25. Alamro, F.S.; Hefnawy, M.A.; Nafee, S.S.; Al-Kadhi, N.S.; Pashameah, R.A.; Ahmed, H.A.; Medany, S.S. Chitosan Supports Boosting $NiCo_2O_4$ for Catalyzed Urea Electrochemical Removal Application. *Polymers* **2023**, *15*, 3058. [CrossRef] [PubMed]
26. Ding, R.; Qi, L.; Jia, M.; Wang, H. Facile synthesis of mesoporous spinel $NiCo_2O_4$ nanostructures as highly efficient electrocatalysts for urea electro-oxidation. *Nanoscale* **2014**, *6*, 1369–1376. [CrossRef] [PubMed]
27. Sha, L.; Ye, K.; Wang, G.; Shao, J.; Zhu, K.; Cheng, K.; Yan, J.; Wang, G.; Cao, D. Hierarchical $NiCo_2O_4$ nanowire array supported on Ni foam for efficient urea electrooxidation in alkaline medium. *J. Power Sources* **2019**, *412*, 265–271. [CrossRef]
28. Zhan, J.; Cai, M.; Zhang, C.; Wang, C. Synthesis of mesoporous $NiCo_2O_4$ fibers and their electrocatalytic activity on direct oxidation of ethanol in alkaline media. *Electrochim. Acta* **2015**, *154*, 70–76. [CrossRef]
29. Almeida, T.S.; Garbim, C.; Silva, R.G.; De Andrade, A.R. Addition of iron oxide to Pt-based catalyst to enhance the catalytic activity of ethanol electrooxidation. *J. Electroanal. Chem.* **2017**, *796*, 49–56. [CrossRef]
30. Hefnawy, M.A.; Medany, S.S.; El-Sherif, R.M.; Fadlallah, S.A. Green synthesis of NiO/Fe_3O_4@chitosan composite catalyst based on graphite for urea electro-oxidation. *Mater. Chem. Phys.* **2022**, *290*, 126603. [CrossRef]
31. Aksaray, G.; Mert, M.E.; Mert, B.D.; Kardaş, G. Catalytic insights into methanol electrooxidation on Ni foam modified with Bi_2O_3-Acetylene black-rGO: Synthesis, characterization, and performance evaluation. *Int. J. Hydrogen Energy* 2024, *article in press*. [CrossRef]
32. Wei, Z.; Wang, Q.; Qu, M.; Zhang, H. Rational Design of Nanosheet Array-Like Layered-Double-Hydroxide-Derived $NiCo_2O_4$ In Situ Grown on Reduced-Graphene-Oxide-Coated Nickel Foam for High-Performance Solid-State Supercapacitors. *ACS Appl. Mater. Interfaces* **2024**, *16*, 18734–18744. [CrossRef] [PubMed]
33. Tsai, M.-H.; Chen, T.-C.; Juang, Y.; Hua, L.-C.; Huang, C. High catalytic performance of CuCo/nickel foam electrode for ammonia electrooxidation. *Electrochem. Commun.* **2020**, *121*, 106875. [CrossRef]
34. Liang, Y.; Liu, Q.; Asiri, A.M.; Sun, X. Enhanced electrooxidation of urea using $NiMoO_4 \cdot xH_2O$ nanosheet arrays on Ni foam as anode. *Electrochim. Acta* **2015**, *153*, 456–460. [CrossRef]
35. Chen, C.; Wen, H.; Tang, P.-P.; Wang, P. Supported Ni@Ni_2P core–shell nanotube Arrays on Ni foam for hydrazine electrooxidation. *ACS Sustain. Chem. Eng.* **2021**, *9*, 4564–4570. [CrossRef]
36. Sha, L.; Ye, K.; Wang, G.; Shao, J.; Zhu, K.; Cheng, K.; Yan, J.; Wang, G.; Cao, D. Rational design of $NiCo_2S_4$ nanowire arrays on nickle foam as highly efficient and durable electrocatalysts toward urea electrooxidation. *Chem. Eng. J.* **2019**, *359*, 1652–1658. [CrossRef]
37. Li, Y.; Hai, Z.; Hou, X.; Xu, H.; Zhang, Z.; Cui, D.; Xue, C.; Zhang, B. Self-Assembly of 3D Fennel-Like Co_3O_4 with Thirty-Six Surfaces for High Performance Supercapacitor. *J. Nanomater.* **2017**, *2017*, 1404328. [CrossRef]
38. Vijayan, S.; Narasimman, R.; Prabhakaran, K. A carbothermal reduction method for the preparation of nickel foam from nickel oxide and sucrose. *Mater. Lett.* **2016**, *181*, 268–271. [CrossRef]
39. Geaney, H.; McNulty, D.; O'Connell, J.; Holmes, J.D.; O'Dwyer, C. Assessing Charge Contribution from Thermally Treated Ni Foam as Current Collectors for Li-Ion Batteries. *J. Electrochem. Soc.* **2016**, *163*, A1805. [CrossRef]
40. Cai, L.; Li, Y.; Xiao, X.; Wang, Y. The electrochemical performances of $NiCo_2O_4$ nanoparticles synthesized by one-step solvothermal method. *Ionics* **2017**, *23*, 2457–2463. [CrossRef]
41. Khalid, S.; Cao, C.; Wang, L.; Zhu, Y. Microwave Assisted Synthesis of Porous $NiCo_2O_4$ Microspheres: Application as High Performance Asymmetric and Symmetric Supercapacitors with Large Areal Capacitance. *Sci. Rep.* **2016**, *6*, 22699. [CrossRef]
42. Waghmode, R.B.; Torane, A.P. Hierarchical 3D $NiCo_2O_4$ nanoflowers as electrode materials for high performance supercapacitors. *J. Mater. Sci. Mater. Electron.* **2016**, *27*, 6133–6139. [CrossRef]
43. Qayoom, M.; Shah, K.A.; Pandit, A.H.; Firdous, A.; Dar, G.N. Dielectric and electrical studies on iron oxide (α-Fe_2O_3) nanoparticles synthesized by modified solution combustion reaction for microwave applications. *J. Electroceram.* **2020**, *45*, 7–14. [CrossRef]
44. Xu, S.; Habib, A.H.; Gee, S.H.; Hong, Y.K.; McHenry, M.E. Spin orientation, structure, morphology, and magnetic properties of hematite nanoparticles. *J. Appl. Phys.* **2015**, *117*, 17A315. [CrossRef]
45. Das, R.; Witanachchi, C.; Nemati, Z.; Kalappattil, V.; Rodrigo, I.; García, J.Á.; Garaio, E.; Alonso, J.; Lam, V.D.; Le, A.-T.; et al. Magnetic Vortex and Hyperthermia Suppression in Multigrain Iron Oxide Nanorings. *Appl. Sci.* **2020**, *10*, 787. [CrossRef]

46. Li, X.; Wei, W.; Wang, S.; Kuai, L.; Geng, B. Single-crystalline α-Fe_2O_3 oblique nanoparallelepipeds: High-yield synthesis, growth mechanism and structure enhanced gas-sensing properties. *Nanoscale* **2011**, *3*, 718–724. [CrossRef] [PubMed]
47. Grosvenor, A.P.; Biesinger, M.C.; Smart, R.S.C.; McIntyre, N.S. New interpretations of XPS spectra of nickel metal and oxides. *Surf. Sci.* **2006**, *600*, 1771–1779. [CrossRef]
48. Hengne, A.M.; Samal, A.K.; Enakonda, L.R.; Harb, M.; Gevers, L.E.; Anjum, D.H.; Hedhili, M.N.; Saih, Y.; Huang, K.-W.; Basset, J.-M. Ni–Sn-Supported ZrO_2 Catalysts Modified by Indium for Selective CO_2 Hydrogenation to Methanol. *ACS Omega* **2018**, *3*, 3688–3701. [CrossRef] [PubMed]
49. Hu, X.; Tian, X.; Lin, Y.-W.; Wang, Z. Nickel foam and stainless steel mesh as electrocatalysts for hydrogen evolution reaction, oxygen evolution reaction and overall water splitting in alkaline media. *RSC Adv.* **2019**, *9*, 31563–31571. [CrossRef] [PubMed]
50. Ma, J.; Guo, E.; Yin, L. Porous hierarchical spinel Mn-doped $NiCo_2O_4$ nanosheet architectures as high-performance anodes for lithium-ion batteries and electrochemical reaction mechanism. *J. Mater. Sci. Mater. Electron.* **2019**, *30*, 8555–8567. [CrossRef]
51. Tong, X.; Pang, N.; Qu, Y.; Yan, C.; Xiong, D.; Xu, S.; Wang, L.; Chu, P.K. 3D urchin-like $NiCo_2O_4$ coated with carbon nanospheres prepared on flexible graphite felt for efficient bifunctional electrocatalytic water splitting. *J. Mater. Sci.* **2021**, *56*, 9961–9973. [CrossRef]
52. Liu, Y.; Liu, P.; Qin, W.; Wu, X.; Yang, G. Laser modification-induced NiCo2O4-δ with high exterior Ni^{3+}/Ni^{2+} ratio and substantial oxygen vacancies for electrocatalysis. *Electrochim. Acta* **2019**, *297*, 623–632. [CrossRef]
53. Mi, L.; Wei, W.; Huang, S.; Cui, S.; Zhang, W.; Hou, H.; Chen, W. A nest-like Ni@Ni 1.4 $Co_{1.6}S_2$ electrode for flexible high-performance rolling supercapacitor device design. *J. Mater. Chem. A* **2015**, *3*, 20973–20982. [CrossRef]
54. Marco, J.F.; Gancedo, J.R.; Gracia, M.; Gautier, J.L.; Ríos, E.; Berry, F.J. Characterization of the nickel cobaltite, $NiCo_2O_4$, prepared by several methods: An XRD, XANES, EXAFS, and XPS study. *J. Solid State Chem.* **2000**, *153*, 74–81. [CrossRef]
55. Gwag, J.-S.; Sohn, Y.-K. Interfacial natures and controlling morphology of Co oxide nanocrystal structures by adding spectator Ni ions. *Bull. Korean Chem. Soc.* **2012**, *33*, 505–510. [CrossRef]
56. Fierro, J.L.G.; Pena, M.A.; González Tejuca, L. An XPS and reduction study of $PrCoO_3$. *J. Mater. Sci.* **1988**, *23*, 1018–1023. [CrossRef]
57. Kim, K.S.; Davis, R.E. 1-Electron spectroscopy of the nickel-oxygen system. *J. Electron Spectros. Relat. Phenom.* **1972**, *1*, 251–258. [CrossRef]
58. Kim, Y.J.; Park, C.R. Analysis of problematic complexing behavior of ferric chloride with N, N-dimethylformamide using combined techniques of FT-IR, XPS, and TGA/DTG. *Inorg. Chem.* **2002**, *41*, 6211–6216. [CrossRef] [PubMed]
59. Allen, G.C.; Curtis, M.T.; Hooper, A.J.; Tucker, P.M. X-ray photoelectron spectroscopy of iron–oxygen systems. *J. Chem. Soc. Dalt. Trans.* **1974**, *14*, 1525–1530. [CrossRef]
60. Li, J.; Wang, Y.; Xu, W.; Wang, Y.; Zhang, B.; Luo, S.; Zhou, X.; Zhang, C.; Gu, X.; Hu, C. Porous Fe_2O_3 nanospheres anchored on activated carbon cloth for high-performance symmetric supercapacitors. *Nano Energy* **2019**, *57*, 379–387. [CrossRef]
61. Mallick, S.; Jana, P.P.; Raj, C.R. Asymmetric supercapacitor based on chemically coupled hybrid material of Fe_2O_3-Fe_3O_4 heterostructure and nitrogen-doped reduced graphene oxide. *ChemElectroChem* **2018**, *5*, 2348–2356. [CrossRef]
62. Zhong, B.; Wang, C.; Yu, Y.; Xia, L.; Wen, G. Facile fabrication of carbon microspheres decorated with B(OH)3 and α-Fe_2O_3 nanoparticles: Superior microwave absorption. *J. Colloid Interface Sci.* **2017**, *505*, 402–409. [CrossRef]
63. Mohapatra, S.; Pal, D.; Ghosh, S.K.; Pramanik, P. Design of superparamagnetic iron oxide nanoparticle for purification of recombinant proteins. *J. Nanosci. Nanotechnol.* **2007**, *7*, 3193–3199. [CrossRef] [PubMed]
64. Ketteler, G.; Yamamoto, S.; Bluhm, H.; Andersson, K.; Starr, D.E.; Ogletree, D.F.; Ogasawara, H.; Nilsson, A.; Salmeron, M. The nature of water nucleation sites on TiO_2(110) surfaces revealed by ambient pressure X-ray photoelectron spectroscopy. *J. Phys. Chem. C* **2007**, *111*, 8278–8282. [CrossRef]
65. Mitchell, C.E.; Santos-Carballal, D.; Beale, A.M.; Jones, W.; Morgan, D.J.; Sankar, M.; de Leeuw, N.H. The role of surface oxidation and Fe–Ni synergy in Fe–Ni–S catalysts for CO_2 hydrogenation. *Faraday Discuss.* **2021**, *230*, 30–51. [CrossRef] [PubMed]
66. Li, L.; Ma, P.; Hussain, S.; Jia, L.; Lin, D.; Yin, X.; Lin, Y.; Cheng, Z.; Wang, L. FeS2/carbon hybrids on carbon cloth: A highly efficient and stable counter electrode for dye-sensitized solar cells. *Sustain. Energy Fuels* **2019**, *3*, 1749–1756. [CrossRef]
67. Yamashita, T.; Hayes, P. Analysis of XPS spectra of Fe^{2+} and Fe^{3+} ions in oxide materials. *Appl. Surf. Sci.* **2008**, *254*, 2441–2449. [CrossRef]
68. Hefnawy, M.A.; Medany, S.S.; El-Sherif, R.M.; El-Bagoury, N.; Fadlallah, S.A. High-performance IN738 superalloy derived from turbine blade waste for efficient ethanol, ethylene glycol, and urea electrooxidation. *J. Appl. Electrochem.* **2023**, *53*, 1337–1348. [CrossRef]
69. Hasan, M.; Newcomb, S.B.; Razeeb, K.M. Porous core/shell Ni@NiO/Pt hybrid nanowire arrays as a high efficient electrocatalyst for alkaline direct ethanol fuel cells. *J. Electrochem. Soc.* **2012**, *159*, F203. [CrossRef]
70. Ahmed, M.S.; Jeon, S. Synthesis and Electrocatalytic Activity Evaluation of Nanoflower Shaped Ni-Pd on Alcohol Oxidation Reaction. *J. Electrochem. Soc.* **2014**, *161*, F1300. [CrossRef]
71. Wang, W.; Li, X.; Cheng, Y.; Zhang, M.; Zhao, K.; Liu, Y. An effective PtPdAuCuFe/C high-entropy-alloy applied to direct ethylene glycol fuel cells. *J. Taiwan Inst. Chem. Eng.* **2023**, *143*, 104714. [CrossRef]
72. Hefnawy, M.A.; Fadlallah, S.A.; El-Sherif, R.M.; Medany, S.S. Synergistic effect of Cu-doped NiO for enhancing urea electrooxidation: Comparative electrochemical and DFT studies. *J. Alloys Compd.* **2021**, *896*, 162857. [CrossRef]

73. Hefnawy, M.A.; Medany, S.S.; El-Sherif, R.M.; Fadlallah, S.A. NiO-MnOx/Polyaniline/Graphite Electrodes for Urea Electrocatalysis: Synergetic Effect between Polymorphs of MnOx and NiO. *ChemistrySelect* **2022**, *7*, e202103735. [CrossRef]
74. Xu, C.; Shen, P.K.; Ji, X.; Zeng, R.; Liu, Y. Enhanced activity for ethanol electrooxidation on Pt–MgO/C catalysts. *Electrochem. Commun.* **2005**, *7*, 1305–1308. [CrossRef]
75. Yu, Z.; Xu, J.; Amorim, I.; Li, Y.; Liu, L. Easy preparation of multifunctional ternary PdNiP/C catalysts toward enhanced small organic molecule electro-oxidation and hydrogen evolution reactions. *J. Energy Chem.* **2021**, *58*, 256–263. [CrossRef]
76. Ramulifho, T.; Ozoemena, K.I.; Modibedi, R.M.; Jafta, C.J.; Mathe, M.K. Electrocatalytic oxidation of ethylene glycol at palladium-bimetallic nanocatalysts (PdSn and PdNi) supported on sulfonate-functionalised multi-walled carbon nanotubes. *J. Electroanal. Chem.* **2013**, *692*, 26–30. [CrossRef]
77. Yang, X.; Yuan, Q.; Sheng, T.; Wang, X. Mesoporous Mo-doped PtBi intermetallic metallene superstructures to enable the complete electrooxidation of ethylene glycol. *Chem. Sci.* **2024**, *15*, 4349–4357. [CrossRef] [PubMed]
78. Basumatary, P.; Lee, U.H.; Konwar, D.; Yoon, Y.S. An efficient tri-metallic anodic electrocatalyst for urea electro-oxidation. *Int. J. Hydrogen Energy* **2020**, *45*, 32770–32779. [CrossRef]
79. Wu, F.; Eid, K.; Abdullah, A.M.; Niu, W.; Wang, C.; Lan, Y.; Elzatahry, A.A.; Xu, G. Unveiling one-pot template-free fabrication of exquisite multidimensional PtNi multicube nanoarchitectonics for the efficient electrochemical oxidation of ethanol and methanol with a great tolerance for CO. *ACS Appl. Mater. Interfaces* **2020**, *12*, 31309–31318. [CrossRef] [PubMed]
80. Forslund, R.P.; Mefford, J.T.; Hardin, W.G.; Alexander, C.T.; Johnston, K.P.; Stevenson, K.J. Nanostructured $LaNiO_3$ perovskite electrocatalyst for enhanced urea oxidation. *ACS Catal.* **2016**, *6*, 5044–5051. [CrossRef]
81. Hefnawy, M.A.; Fadlallah, S.A.; El-Sherif, R.M.; Medany, S.S. Systematic DFT studies of CO-Tolerance and CO oxidation on Cu-doped Ni surfaces. *J. Mol. Graph. Model.* **2023**, *118*, 108343. [CrossRef]
82. Foroutan Koudahi, M.; Naji, L. Hydrothermal synthesis of nickel foam-supported spinel $ZnNi_2O_4$ nanostructure as electrode materials for supercapacitors. *Electrochim. Acta* **2022**, *434*, 141314. [CrossRef]
83. Ispas, A.; Matsushima, H.; Plieth, W.; Bund, A. Influence of a magnetic field on the electrodeposition of nickel–iron alloys. *Electrochim. Acta* **2007**, *52*, 2785–2795. [CrossRef]
84. Yin, K.-M.; Lin, B.-T. Effects of boric acid on the electrodeposition of iron, nickel and iron-nickel. *Surf. Coat. Technol.* **1996**, *78*, 205–210. [CrossRef]